© 2020. Published by The Company of Biologists Ltd | Journal of Cell Science (2020) 133, jcs240648. doi:10.1242/jcs.240648

RESEARCH ARTICLE

Epb41l5 interacts with Iqcb1 and regulates ciliary function in zebrafish embryos

Tiffany Yu[1] and Miho Matsuda[1,2,*]

ABSTRACT

Erythrocyte protein band 4.1 like 5 (EPB41L5) is an adaptor protein beneath the plasma membrane that functions to control epithelial morphogenesis. Here we report a previously uncharacterized role of EPB41L5 in controlling ciliary function. We found that EPB41L5 forms a complex with IQCB1 (previously known as NPHP5), a ciliopathy protein. Overexpression of EPB41L5 reduced IQCB1 localization at the ciliary base in cultured mammalian epithelial cells. Conversely, *epb41l5* knockdown increased IQCB1 localization at the ciliary base. *epb41l5*-deficient zebrafish embryos or embryos expressing C-terminally modified forms of Epb41l5 developed cilia with reduced motility and exhibited left–right patterning defects, an outcome of abnormal ciliary function. We observed genetic synergy between *epb41l5* and *iqcb1*. Moreover, EPB41L5 decreased IQCB1 interaction with CEP290, another ciliopathy protein and a component of the ciliary base and centrosome. Together, these observations suggest that EPB41L5 regulates the composition of the ciliary base and centrosome through IQCB1 and CEP290.

KEY WORDS: Cilia, Epithelial morphogenesis, Zebrafish, Left–right patterning, EPB41L5, IQCB1

INTRODUCTION

Cilia are antenna-like structures that extend from the surface of the apical membrane of cells and play important roles in sensing a variety of extracellular signals (Carvalho-Santos et al., 2011; Ishikawa, 2017; Loreng and Smith, 2017; Pazour and Witman, 2003). Cilia-mediated signaling regulates cell proliferation, differentiation and function, and plays essential roles in embryonic development and tissue homeostasis in adults (D'Angelo and Franco, 2009; Goetz and Anderson, 2010; Tasouri and Tucker, 2011). Defects in ciliary structure and function lead to a number of human diseases called ciliopathies (Avasthi et al., 2017; Cao et al., 2010; Dell, 2015; Estrada-Cuzcano et al., 2012; Hildebrandt et al., 2009; Kagan et al., 2017; Klena et al., 2017; Oud et al., 2017).

Ciliogenesis is initiated by the formation of membrane vesicles at the distal end of the mother centriole (Mirvis et al., 2018; Nigg and Raff, 2009). The centrosome migrates to the apical cell cortex where the mother centriole transforms into the basal body and initiates assembly of the axoneme (Avidor-Reiss et al., 2017; Bernabé-Rubio and Alonso, 2017; Linck et al., 2016). Intraflagellar transport (IFT) mediates bi-directional transport of cargo proteins in and out of the cilia (Ishikawa and Marshall, 2017; Kim et al., 2010; Li and Hu, 2011; Pedersen and Rosenbaum, 2008). This cargo includes various structural components of the cilia and proteins crucial for signal transduction (Corbit et al., 2005, 2008; Madhivanan and Aguilar, 2014; Nachury, 2014; Wheway et al., 2018).

Cilia have a specialized domain at the base of the cilium, named the ciliary transition zone (TZ). The TZ is an ultrastructurally defined complex barrier that acts as a gate to control protein entry and exit from the cilia. The ciliary transport is highly selective, which enables the establishment of a unique composition of soluble and membrane proteins in the cilia. Previous studies have identified multiple TZ components, many of which are encoded by the genes responsible for Meckel–Gruber syndrome (MKS) (Barker et al., 2014; Dawe et al., 2007; Kagan et al., 2017; Williams et al., 2011; Zhao and Malicki, 2011), Joubert syndrome (Garcia-Gonzalo et al., 2011; Kagan et al., 2017; Lee et al., 2012; Mitchison and Valente, 2017; Romani et al., 2013) and nephronophthisis (NPHP) (Chih et al., 2012; Craige et al., 2010; Garcia-Gonzalo et al., 2011; Kee et al., 2012; Sang et al., 2011; Williams et al., 2011). NPHP and MKS proteins form modules and cooperate to establish the TZ and compartmentalize the ciliary domain (Avidor-Reiss et al., 2017; Chih et al., 2012; Garcia-Gonzalo et al., 2011; Gonçalves and Pelletier, 2017; Takao et al., 2017; Williams et al., 2011). Although the importance of the TZ for cilia has been established, it is largely unknown how the TZ is specified, organized and maintained.

Erythrocyte protein band 4.1 like 5 (EPB41L5) is an adaptor protein that contains the FERM (band 4.1, ezrin, radixin and moesin) domain (Baines, 2006; Moleirinho et al., 2013; Tepass, 2009) and regulates morphogenesis of epithelial and neuroepithelial cells. First, EPB41L5 functions in apico-basal polarity by modulating the distribution of Crumbs at the apical membrane (Christensen and Jensen, 2008; Gamblin et al., 2018; Gosens et al., 2007; Hoover and Bryant, 2002; Hsu et al., 2006; Jensen et al., 2001; Jensen and Westerfield, 2004; Laprise et al., 2006; Perez-Vale and Peifer, 2018). Second, EPB41L5 is required for disassembly of cadherin-based adherens junctions to promote epithelial-to-mesenchymal transition (Hirano et al., 2008; Lee et al., 2007) and apical detachment of differentiating neurons (Matsuda et al., 2016). Third, EPB41L5 is involved in the formation and maintenance of focal adhesion in podocytes in adult mice (Hirano et al., 2008; Schell et al., 2017). Furthermore, EPB41L5 has also been shown to induce apical constriction in cultured epithelial cells (Nakajima and Tanoue, 2010, 2011) and *Xenopus* ectoderm (Chu et al., 2013). In this manner, EPB41L5 plays diverse functions in epithelial morphogenesis and its functional diversity might be determined by its partner proteins and/or cell types.

Although EPB41L5 does not interact with actin directly, EPB41L5 appears to play roles in modulating organization of

[1]Department of Cell Biology and Molecular Medicine, Rutgers New Jersey Medical School, Newark, NJ 07302, USA. [2]Department of Cell, Developmental and Regenerative Biology, Icahn School of Medicine at Mount Sinai, New York, NY 10029, USA.

*Author for correspondence (miho.matsuda@mssm.edu)

M.M., 0000-0002-7495-5905

Handling Editor: David Stephens
Received 21 October 2019; Accepted 13 May 2020

Journal of Cell Science (2020) 133, jcs240648. doi:10.1242/jcs.240648

the actin cytoskeleton, in particular actin at the apical or sub-apical cortex. Indeed, EPB41L5 interacts with actin modifiers, including p114RhoGEF (Nakajima and Tanoue, 2010, 2011; Schell et al., 2017) and vimentin (Hirano et al., 2008). However, it remains incompletely understood how EPB41L5 modulates actin networks for epithelial morphogenesis.

In this study, we report that EPB41L5 interacts with IQ calmodulin-binding motif-containing 1 [IQCB1, also called nephrocystin 5 (NPHP5)]. IQCB1 has been implicated in nephronophthisis, an autosomal recessive cystic kidney disease (Barbelanne et al., 2013; Downs et al., 2016; Hildebrandt et al., 2009; Otto et al., 2005; Schäfer et al., 2008; Stone et al., 2011). We show that EPB41L5 suppresses IQCB1 accumulation at the ciliary base in ciliated hTERT-RPE1 cells and at the centrosome in non-ciliated cells. We also show that zebrafish embryos deficient in *epb41l5* and embryos expressing the C-terminally modified Epb41l5 have ciliary dysfunction. Furthermore, we demonstrate that EPB41L5 reduces IQCB1 interaction with centrosomal protein 290 (CEP290, previously known as NPHP6) in HEK293 cells. Taken together, we propose that EPB41L5 controls the integrity of the ciliary base and centrosome through IQCB1 and CEP290.

RESULTS

Identification of IQCB1 as a novel interacting protein of EPB41L5

To identify EPB41L5-interacting proteins, we conducted mass spectrometry analysis of proteins physically interacting with EPB41L5. IQCB1 was identified by immunoprecipitation of mouse EPB41L5 expressed in HEK293 cells. IQCB1 contains three IQ calmodulin-binding motifs, one coiled-coil domain and a CEP290-interacting domain at the C terminus (Fig. 1B) (Barbelanne et al., 2013). We confirmed interaction between EPB41L5 and IQCB1 by co-immunoprecipitation of myc-tagged zebrafish or mouse EPB41L5 and FLAG- or HA-tagged human IQCB1 (Fig. 1C,D).

We next identified protein domains involved in the interaction between EPB41L5 and IQCB1 (Fig. 1A,B). We found that the N-terminal FERM domain of zebrafish Epb41l5 (amino acids 1–239) was required and sufficient for Epb41l5 binding to IQCB1 (Fig. 1C). Removing the C-terminal conserved domain of Epb41l5 (Epb41l5ΔCTD) increased Epb41l5 binding to IQCB1 (Fig. 1C), suggesting that the CTD inhibits Epb41l5–IQCB1 interaction. Lack of a strong signal in co-immunoprecipitation of the full-length Epb41l5 protein might also be a result of its poor stability (Matsuda et al., 2016). On the other hand, the internal domain of IQCB1 containing three IQ motifs and a coiled-coil domain (amino acids 287–443) was required and sufficient for the Epb41l5–IQCB1 interaction (Fig. 1D). Taken together, these results suggest that EPB41L5 interacts with IQCB1 via the FERM domain of Epb41l5 and the IQ-coiled coil domain of IQCB1.

EPB41L5 suppresses IQCB1 localization at the ciliary base

We next asked whether EPB41L5 and IQCB1modulate each other's subcellular localization. As previously reported (Hirano et al., 2008; Matsuda et al., 2016; Nakajima and Tanoue, 2010, 2011), FLAG-tagged Epb41l5 is associated with the plasma membrane in hTERT-RPE1 cells (Fig. 2A) and with the basolateral membrane of polarized Madin–Darby canine kidney (MDCK) epithelial cells (Fig. S1A,A″). When IQCB1 and Epb41l5 were coexpressed, IQCB1 did not alter Epb41l5 localization in either hTERT-RPE1 cells (Fig. 2C′) or MDCK cells (Fig. S1C,C″).

By contrast, Epb41l5 modified IQCB1 localization. We observed that HA-tagged IQCB1 accumulated at the base of cilia marked by the ciliary protein ARL13B and in cytoplasmic puncta (Fig. 2B; Fig. S1B–B″), which is consistent with previous observations (Barbelanne et al., 2015, 2013; Das et al., 2017). We note that the immunostaining of endogenous IQCB1 using a commercial anti-IQCB1 antibody was below the detection limit (data not shown). Coexpression of Epb41l5 reduced IQCB1 accumulation at the ciliary base (Fig. 2C,F). Conversely, *epb41l5* knockdown by short hairpin RNA (shRNA; Fig. 2E) further enriched cilium-associated IQCB1 immunostaining (Fig. 2D,G). We confirmed that coexpression of exogenous Epb41l5 rescued the accumulation of IQCB1 at the ciliary base in *epb41l5* knocked-down cells (Fig. 2G). Taken together, these results suggest that EPB41L5 suppresses IQCB1 localization at the ciliary base.

EPB41L5 binding to the IQ-coiled-coil domain suppresses IQCB1 localization at the ciliary base

We sought to understand how EPB41L5 suppresses IQCB1 localization at the ciliary base. A previous study showed that the coiled-coil domain of IQCB1 was involved in IQCB1 localization at the centrosome (Barbelanne et al., 2013), which develops into the ciliary base. We showed that EPB41L5 binds to IQCB1 through the region containing the coiled-coil domain (Fig. 1D). This raised the possibility that EPB41L5 competitively inhibits IQCB1 association with the ciliary base. Consistent with this hypothesis, coexpression of the N-terminal FERM-FA domain of Epb41l5 [Epb41l5(FERM-FA)] was sufficient to reduce IQCB1 accumulation at the ciliary base (Fig. 3A). The efficacy of the suppression might be stronger than full-length Epb41l5 (Fig. 2F). Coexpression of the C-terminal fragment of Epb41l5 [Epb41l5(Cfrag)] did not change IQCB1 accumulation at the ciliary base (Fig. 3B). These results suggest that EPB41L5 binding to IQCB1 suppresses IQCB1 localization at the ciliary base.

Next, we investigated whether the domain between amino acids 287 and 443 was required for IQCB1 displacement from the ciliary base. As described in a previous study (Barbelanne et al., 2013), ciliogenesis was impaired in cells expressing IQCB1Δ(287–443) (Fig. 3C′). Therefore, we examined IQCB1 association with the centrosome. First, we confirmed that IQCB1Δ(287–443) showed colocalization with centrosomal proteins γ-tubulin (Fig. S2A) and NEDD1 (Fig. S2B), as well as ARL13B (Fig. 3C). For this analysis, we used ARL13B as a centrosomal marker to make this more comparable with analyses of other IQCB1 deletion mutant proteins. It should be noted that IQCB1Δ(287–443) association with the centrosome was weaker than that of full-length IQCB1 (Fig. 3C,C″). IQCB1(287–443) did not show accumulation at the centrosome (Fig. 3E,E″). These observations confirm the previous observation that the CEP290-binding domain at the C terminus is important for IQCB1 localization to the centrosome (Barbelanne et al., 2013; Stone et al., 2011). Nevertheless, IQCB1Δ(287–443) accumulation at the centrosome was not altered by EPB41L5 overexpression (Fig. 3D,F). Taken together, these results suggest that EPB41L5 binding to the IQ-coiled-coil domain suppresses centrosomal association of IQCB1.

Abnormal cilia function in *epb41l5*-deficient zebrafish embryos

We next looked at whether Epb41l5 has a regulatory role in cilia formation or function *in vivo* using zebrafish embryos. First, we analyzed cilia formation in *epb41l5*-deficient embryos. We used an *epb41l5* translation blocking morpholino (*epb41l5*-MO^{ATG}) (Hsu et al., 2006; Jensen and Westerfield, 2004; Matsuda et al., 2016) for

Journal of Cell Science (2020) 133, jcs240648. doi:10.1242/jcs.240648

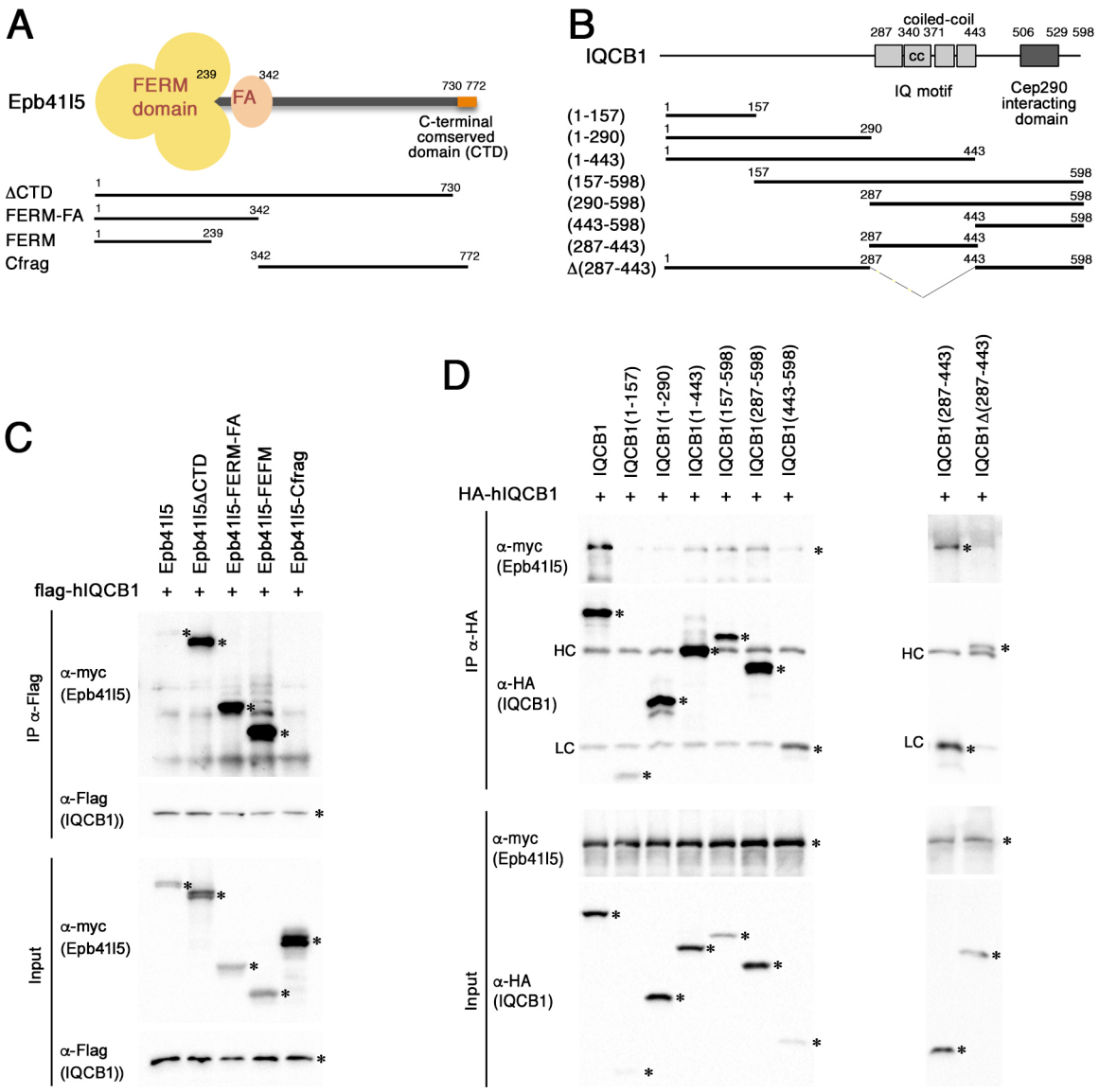

Fig. 1. EPB41L5 interaction with IQCB1. (A) The domain structure of EPB41L5 and deletion constructs used in this study. EPB41L5 contains the FERM and FA domains at the N terminus, and the evolutionarily conserved domain (CTD) at the C terminus. (B) The domain structure of IQCB1 and deletion constructs used in this study. IQCB1 contains three IQ motifs, one coiled-coil domain (CC) and the CEP290-interacting domain at the C terminus. (C) Identification of a domain in Epb41l5 required for its interaction with IQCB1. Myc-Epb41l5 and FLAG-IQCB1 were transiently expressed in HEK293 cells. After 24 h, cell lysates were immunoprecipitated by anti-FLAG antibody. The N-terminal FERM domain of Epb41l5 was required and sufficient for its interaction with IQCB1. Bands corresponding to these exogenously expressed proteins are marked by asterisks. (D) Identification of a domain in IQCB1 required for its interaction with EPB41L5. Myc-EPB41L5 and HA-IQCB1 were transiently expressed in HEK293 cells. After 24 h, cell lysates were immunoprecipitated by anti-HA antibody. The domain between amino acids 287 and 443 was required and sufficient for its interaction with EPB41L5. Bands corresponding to these proteins are marked by asterisks. HC, heavy chain; LC, light chain.

embryos younger than 18 h post fertilization (hpf), because homozygous *moe*^{b476} mutants are not identifiable either genetically or morphologically at 18 hpf or earlier. Also, translation blocking morpholinos are effective at minimizing the effects of maternally loaded *epb41l5* transcripts in embryos. For embryos older than 18 hpf, we used *epb41l5* null mutants *mosaic eyes* (*moe*) (Hsu et al., 2006; Jensen et al., 2001; Jensen and Westerfield, 2004; Kramer-Zucker et al., 2005b). Cilia formation was assessed by immunostaining.

We found that cilia were formed in the pronephric duct in *moe*^{b476} mutants (Fig. 4A–B′) and Kupffer's vesicle (KV) in *epb41l5*-MO^{ATG} morphants (Fig. 4C–F). The presence of cilia in *epb41l5* deficient embryos was expected because *epb41l5* overexpression or knockdown did not alter cilia formation in hTERT-RPE1 cells (Fig. 2A,D) or in MDCK cells (data not shown). This is also consistent with the presence of nodal cilia in mouse *epb41l5* null mutants (Lee et al., 2007).

However, pronephric cilia in *moe*^{b476} zebrafish mutants differed from those in wild-type siblings. In wild-type embryos, pronephric cilia form bundles (Liu et al., 2007), so that individual cilia are not visibly distinguishable (Fig. 4A,A′). In contrast, individual cilia were easier to distinguish in *moe*^{b476} mutants (Fig. 4B,B′). This suggests that the cilia in *epb41l5*-deficient embryos have defects in their function. Consistent with this, the expression of *spaw*, the first gene asymmetrically expressed in the lateral plate mesoderm (LPM) (Long et al., 2003), was randomized in *epb41l5*-MO^{ATG} morphants

Journal of Cell Science (2020) 133, jcs240648. doi:10.1242/jcs.240648

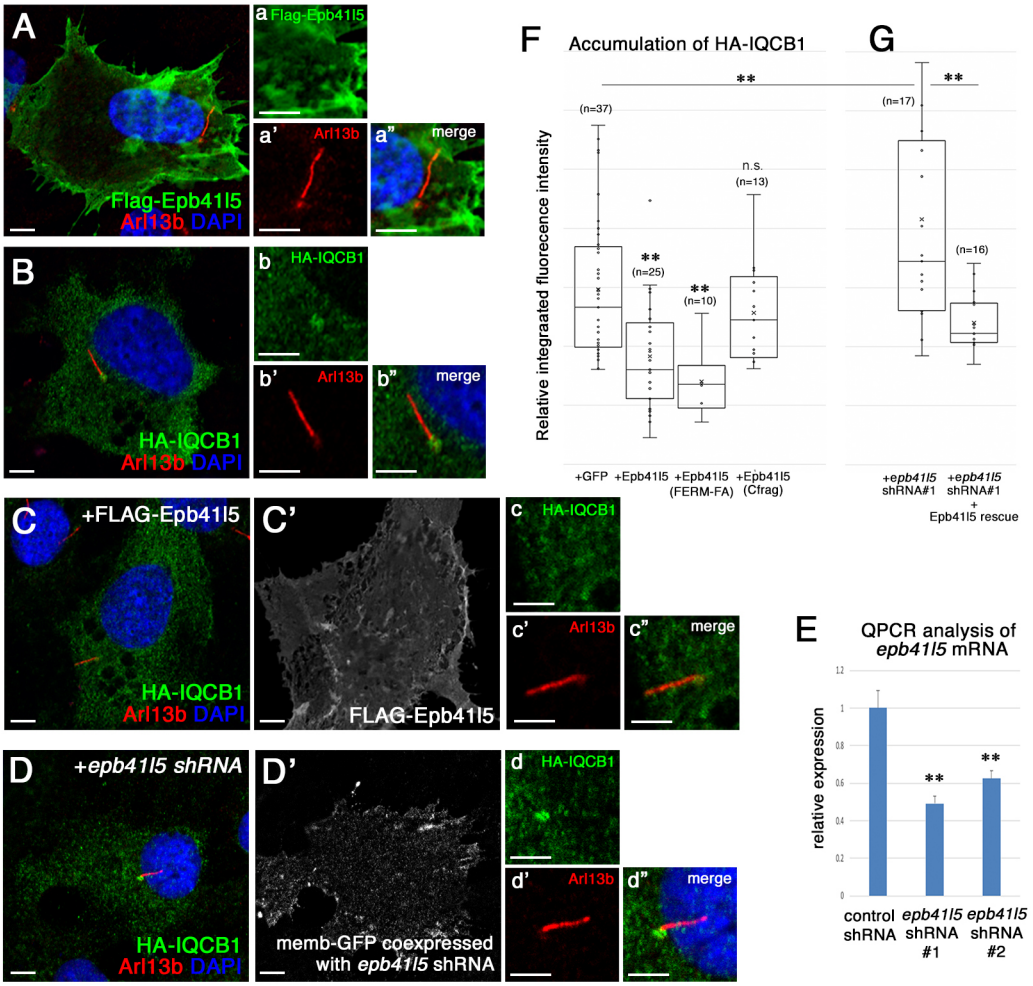

Fig. 2. EPB41L5 suppresses IQCB1 association with the ciliary base in hTERT-RPE1 cells. (A) Subcellular localization of exogenously expressed Epb41l5 in hTERT-RPE1 cells. Epb41l5 was mainly localized at the plasma membrane. Enlarged images of a portion of A are shown in a–a″. Epb41l5 did not colocalize with a ciliary protein ARL13B. (B) Subcellular localization of exogenously expressed IQCB1 in hTERT-RPE1 cells. Enlarged images of a portion of B are shown in b–b″. IQCB1 accumulated at the base of cilia labeled by ARL13B. (C) Coexpression of Epb41l5 reduced accumulation of IQCB1 at the ciliary base. Enlarged images of a portion of C are shown in c–c″ . C′ shows localization of FLAG-Epb41l5. (D) Knockdown of *epb41l5* by shRNA promoted the accumulation of IQCB1 at the ciliary base. shRNA-expressing cells were labeled with GFP. Enlarged images of a portion of D are shown in d–d″. D′ shows expression of memb-GFP as a marker of *epb41l5* shRNA expression. (E) Efficacy of *epb41l5* shRNAs. Two independent *epb41l5* shRNAs were used. *epb41l5* expression was quantified by RT-qPCR. Data are mean±s.d. of n=3 experiments. (F,G) Quantification of HA-IQCB1 accumulation at the ciliary base. HA-IQCB1 was expressed alone or coexpressed with the full-length or deletion mutants of Epb41l5 (F), or coexpressed with *epb41l5* shRNA alone or with exogenous Epb41l5 for shRNA rescue (G). The relative integrated fluorescence intensity in the surrounding area of the ciliary base was quantified using an ImageJ plug-in. Box indicates the interquartile range (IQR) and whiskers indicate inner fences (±1.5×IQR), the horizontal bar shows the median. **P<0.01; n.s., not significant. Scale bars: 5 µm.

(Fig. 4G,H). Cilia are primarily responsible for directional fluid flow generation in KV. Therefore, these results suggest that KV cilia have functional defects, leading to randomized left–right (LR) patterning in *epb41l5*-MO^{ATG} morphants. We also observed randomized cardiac jogging in *epb41l5*-MO^{ATG} morphants, which was rescued by co-injection of *epb41l5* mRNA (Fig. S3). This confirms that LR patterning defects are specific effects of the *epb41l5*-MO^{ATG} morpholino.

Embryos expressing Epb41l5ΔCTD showed largely normal epithelial morphogenesis

Previous studies showed that *epb41l5* deficiency led to severe loss of epithelial integrity in developing zebrafish and mouse embryos (Hsu et al., 2006; Jensen et al., 2001; Jensen and Westerfield, 2004; Lee et al., 2010, 2007; Matsuda et al., 2016). Because cilia form at the apical membrane in epithelial cells, loss of epithelial integrity in *epb41l5*-deficient embryos could alter the spatial distribution of cilia, resulting in cilia dysfunction. Alternatively, EPB41L5 may have a more direct role in cilia, independent of its function on epithelial morphogenesis. In that case, EPB41L5 interaction with IQCB1 might mediate this process.

To explore a more direct role of Epb41l5 in cilia *in vivo*, we analyzed cilia in a novel allele of zebrafish *epb41l5* mutants. The *epb41l5Δctd* mutants were generated using the CRISPR/Cas9 genome engineering system (Chang et al., 2013; Hwang et al., 2013; Li et al., 2016). Three guide RNAs (gRNAs) were designed to target the splicing donor site of exon 25 (Fig. 5A). Indels were confirmed near the gRNA target sites in the genome (Fig. 5B). Exon 25 was spliced out in *epb41l5Δctd* transcripts (Fig. 5C), resulting in a frame-shift and a premature stop codon (Fig. 5D).

Although no *epb41l5* transcripts were detectable in *epb41l5* null mutants *moe*^{b476}, the *epb41l5Δctd* transcripts were present in *epb41l5Δctd* mutants (Fig. 5C), which are expected to produce Epb41l5ΔCTD protein (Fig. 5D). We confirmed that three independent alleles of *epb41l5Δctd* mutants (Fig. 5B) produced

Journal of Cell Science (2020) 133, jcs240648. doi:10.1242/jcs.240648

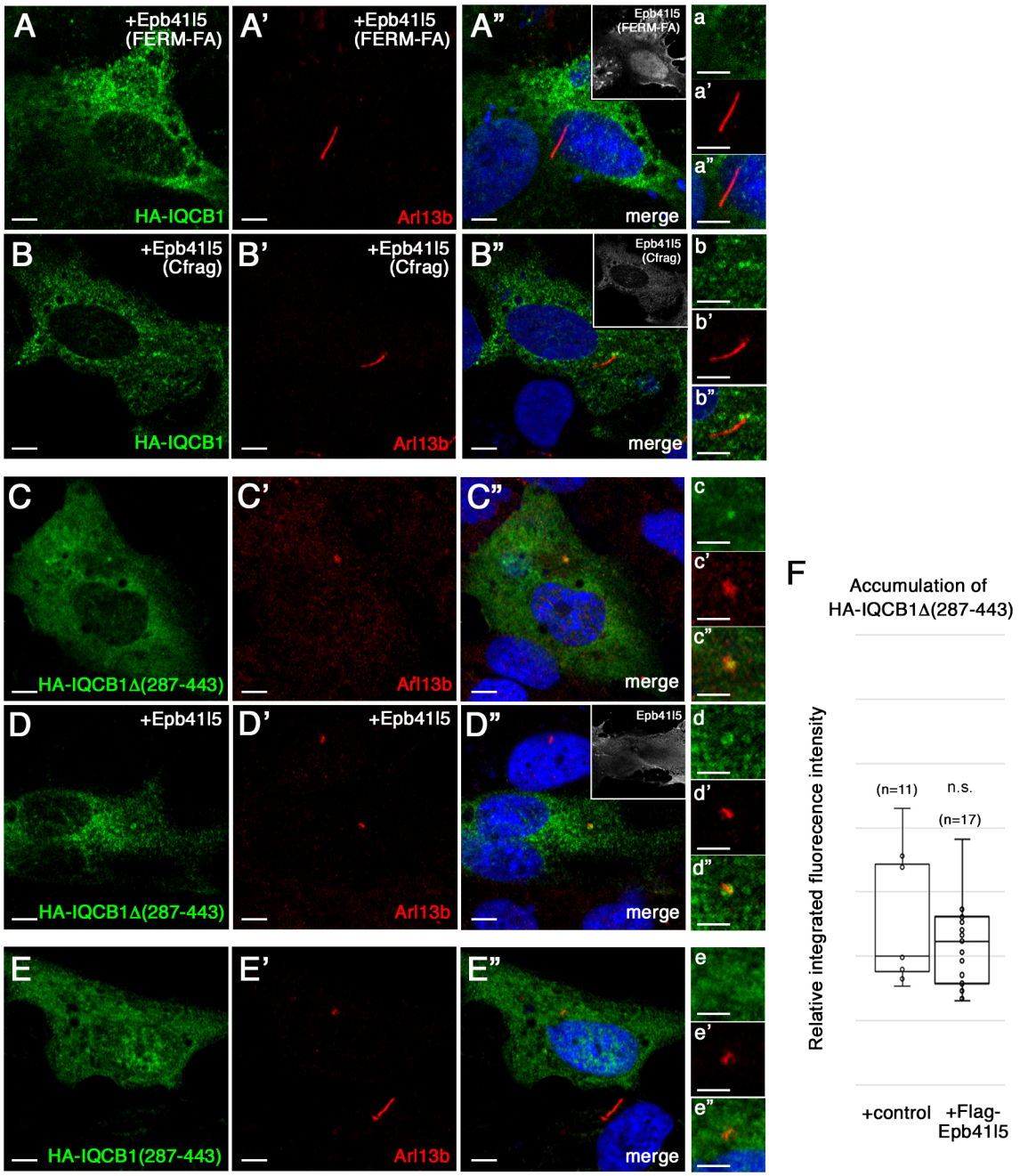

Fig. 3. Identification of domains required for IQCB1 localization control by Epb41l5. (A,B) Full-length IQCB1 was coexpressed with the N-terminal FERM-FA domain of Epb41l5 (A) or the C-terminal fragment of Epb41l5 (B). The accumulation of IQCB1 at the ciliary base was examined. Enlarged images of portions of A–A″ and B–B″ are shown in a–a″ and b–b″, respectively. The N-terminal FERM-FA domain suppressed IQCB1 accumulation at the ciliary base, whereas the C-terminal fragment did not alter IQCB1 localization. (C,D) IQCB1Δ(287–443) was expressed alone (C) or coexpressed with full-length Epb41l5 (D). Enlarged images of portions of C–C″ and D–D″ are shown in c–c″ and d–d″, respectively. Although IQCB1Δ(287–443) accumulated at the ciliary base, Epb41l5 coexpression did not alter the IQCB1Δ (287–443) accumulation. (E) IQCB1(287–443) did not accumulate at the ciliary base. Enlarged images of portions of E–E″ are shown in e–e″. (F) Quantification of IQCB1Δ(287–443) accumulation at the centrosome. IQCB1Δ(287–443) was expressed alone or coexpressed with Epb41l5. The relative integrated fluorescence intensity in the surrounding area of the centrosome was quantified using an ImageJ plug-in. Box indicates the interquartile range (IQR) and whiskers indicate inner fences (±1.5×IQR), the horizontal bar shows the median. n.s., not significant. Scale bars: 5 µm.

the same *epb41l5Δctd* transcripts (data not shown). Importantly, all *epb41l5Δctd* mutants (*epb41l5Δctd1*, *epb41l5Δctd2* and *epb41l5Δctd3*) showed largely normal eye pigmentation, body curvature and brain ventricle inflation (Fig. 5F,I,L), compared with wild-type embryos (Fig. 5E,H,K) and *moe*^{b476} null mutants (Fig. 5G,J,M). These results suggest that epithelial integrity was largely maintained in *epb41l5Δctd* mutants. Unexpectedly, heterozygous *epb41l5Δctd* mutants showed severe male infertility (data not shown). This made it challenging to obtain *epb41l5Δctd* homozygous mutant embryos for further analyses.

Cilia abnormality in embryos expressing Epb41l5ΔCTD

To overcome the limited availability of *epb41l5Δctd* mutants, we took two alternative approaches. First, we designed a morpholino

Journal of Cell Science (2020) 133, jcs240648. doi:10.1242/jcs.240648

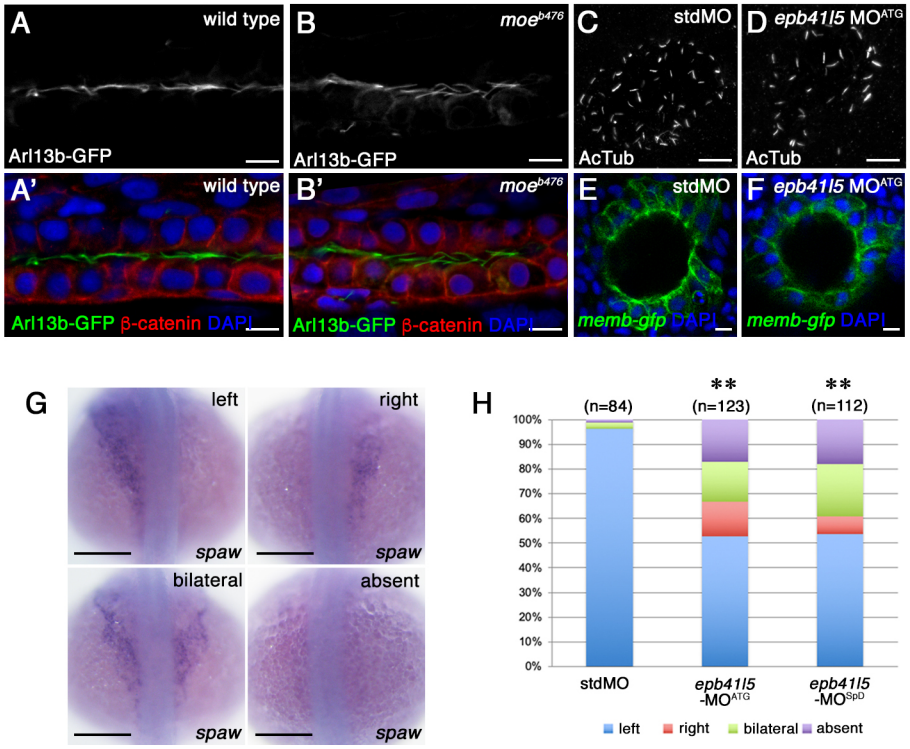

Fig. 4. Abnormal cilia and LR patterning defects in *epb41l5*-deficient embryos. (A,B) Cilia in the pronephric duct in *moe*^{b476} mutants. Cilia and the pronephric epithelium were labeled using GFP-Arl13b and anti-β-catenin immunostaining, respectively. In wild-type embryos, pronephric cilia formed bundles and individual cilia were not distinguishable (A,A′). Although cilia formed in *moe*^{b476} mutants, individual cilia were easier to distinguish (B,B′). (C,D) KV cilia were immunostained with acetylated tubulin (AcTub). Cilia formation was normal in *epb41l5*-MO^{ATG} morphants. (E,F) KV epithelium was labeled with membrane-tethered GFP (memb-GFP) and nuclear dye DAPI. Formation was normal in *epb41l5*-MO^{ATG} morphants. (G,H) Randomized LR patterning in *epb41l5*-MO^{ATG} and *epb41l5*-MO^{SpD} morphants. *spaw* expression was examined by *in situ* hybridization. Individual embryos were scored as either left, right, bilateral or absent. $^{**}P<0.01$. Scale bars: 10 µm (A–F), 200 µm (G).

antisense oligonucleotide (*epb41l5*-MO^{SpD}; Fig. 5A), which targeted the splicing donor site of exon 25. We validated that *epb41l5*-MO^{SpD} injection resulted in the same transcripts as in *epb41l5Δctd* mutants (Fig. 5C). As expected, *epb41l5*-MO^{SpD} morphants did not have significant defects in epithelial morphogenesis, with a largely normal hindbrain ventricle and apical localization of ZO1 at the ventricular surface (Fig. 5O). Second, we overexpressed exogenous Epb41l5 lacking the C-terminal 60 amino acids by mRNA injection (Epb41l5Δ60 in Fig. 5D). The combination of *epb41l5Δctd* mutants, *epb41l5*-MO^{SpD} morphants and embryos expressing exogenous Epb41l5Δ60 helped assess the direct role of Epb41l5 on cilia and reduced the concern for any 'off-target' effect in morphants (Gerety and Wilkinson, 2011; Joris et al., 2017; Kok et al., 2015; Law and Sargent, 2014; Robu et al., 2007; Schulte-Merker and Stainier, 2014; Stainier et al., 2017).

We found that both KV cilia and pronephric cilia formed in *epb41l5*-MO^{SpD} morphants (Fig. 6B,E,E′) and embryos expressing Epb41l5Δ60 (Fig. 6C,F,F′), as was observed in wild-type embryos (Fig. 6A,D,D′). This further confirmed that Epb41l5 is not required for cilia formation. However, cilia appeared to be abnormal in these embryos. In wild-type embryos, individual pronephric cilia were distinguishable because they formed bundles (Fig. 6D,D′). On the other hand, individual pronephric cilia were easier to distinguish in both *epb41l5*-MO^{SpD} morphants (Fig. 6E,E′) and embryos expressing Epb41l5Δ60 (Fig. 6F,F′). This suggests failure of cilia bundle formation in these embryos.

These embryos also showed randomized LR patterning. The direction of cardiac jogging is regulated by LR patterning signals from KV (Amack et al., 2007; Amack and Yost, 2004; Chen et al., 1997; Essner et al., 2005). We found that cardiac jogging was randomized in *epb41l5*-MO^{SpD} morphants (Fig. 6K), *epb41l5Δctd* mutants (Fig. 6L) and embryos expressing Epb41l5Δ60 (Fig. 6M). Randomized cardiac jogging in *epb41l5*-MO^{SpD} morphants was rescued by *epb41l5* mRNA co-injection (Fig. S3), confirming the specificity. Expression of *spaw* was also randomized in the LPM in *epb41l5*-MO^{SpD} morphants (Fig. 4H). *charon* is considered the first asymmetric flow target gene in medaka, zebrafish, frog and mouse (*coco* in frogs and *Cerl2* in mice) (Hashimoto et al., 2004; Hojo et al., 2007; Lopes et al., 2010; Nakamura et al., 2012; Sampaio et al., 2014; Schweickert et al., 2010). We found that *charon* was more symmetrically expressed in *epb41l5*-MO^{SpD} morphants (Fig. 6N,O). Because cilia are primarily responsible for directional fluid flow generation in KV, these results suggest that cilia have motility defects in embryos expressing Epb41l5ΔCTD.

To assess a direct effect of Epb41l5ΔCTD expression on cilia motility, we did live imaging of pronephric cilia in *epb41l5*-MO^{SpD} and *epb41l5*-MO^{ATG} morphants. For live imaging of cilia, *tg[actb:arl13b-gfp]* embryos (Borovina et al., 2010) were imaged on a confocal microscope at 28–30 hpf. Pronephric cilia have been shown to beat at a frequency of 20.0±3.2 Hz in wild-type embryos (Kramer-Zucker et al., 2005a), which is faster than the scanning speed of a conventional confocal microscope. Indeed, individual pronephric cilia were difficult to image in control wild-type embryos (arrowheads in Fig. 6G; Movie 1) as compared to primary cilia in muscle progenitor cells (arrows in Fig. 6G). Notably, pronephric cilia were more clearly captured in *epb41l5*-MO^{ATG} morphants (arrowheads in Fig. 6H; Movie 2) or *epb41l5*-MO^{SpD} morphants (arrowheads in Fig. 6I; Movie 3) than in wild-type embryos (Fig. 6G; Movie 1). This suggests that cilia had reduced motility in *epb41l5*-MO^{ATG} or *epb41l5*-MO^{SpD} morphants. Taken together, these results suggest that Epb41l5 is required for cilia motility. Without normal Epb41l5 function, the ciliary base may lose its integrity, resulting in abnormal cilia motility.

Genetic interactions of Epb41l5 and Iqcb1 in zebrafish embryos

Next, we asked whether Epb41l5 regulates the integrity of the ciliary base together with Iqcb1. To test genetic synergy, we co-injected a small amount of *epb41l5*-MO^{ATG} and *iqcb1* morpholino (Schäfer et al., 2008). First, we confirmed that

Journal of Cell Science (2020) 133, jcs240648. doi:10.1242/jcs.240648

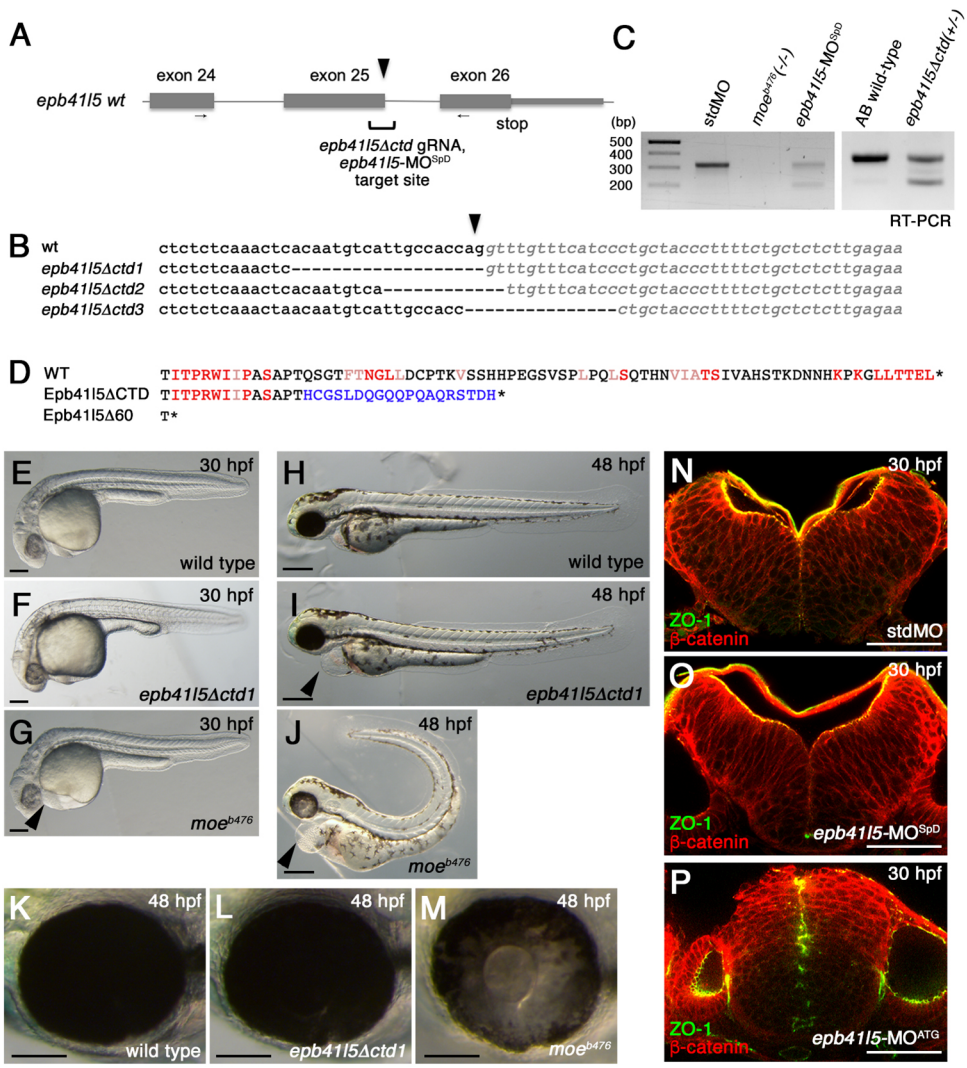

Fig. 5. *epb41l5Δctd* mutants show relatively normal epithelial morphogenesis. (A) Design of *epb41l5Δctd* gRNA and *epb41l5*-MO^{SpD} morpholino. The exon–intron structure of the zebrafish *epb41l5* gene from exon 24 to 26 is shown. The stop codon is located in exon 26. An arrowhead shows the exon–intron boundary of exon 25. Primers used for RT-PCR analysis, shown by arrows, are located in exon 24 and exon 26. (B) Three examples of gene editing in the genome of *epb41l5Δctd* mutants. The exon–intron boundary of exon 25 is shown by an arrowhead. (C) Analysis of *epb41l5* transcripts in homozygous *moe*^{b476} mutant embryos, heterozygous *epb41l5Δctd1* mutant embryos and *epb41l5*-MO^{SpD} morphants. The lower band indicates *epb41l5Δctd* transcripts in which exon 25 is spliced out. All alleles of *epb41l5Δctd* mutants and *epb41l5*-MO^{SpD} morphants generated the same *epb41l5Δctd* transcripts. (D) The predicted protein sequence of Epb41l5ΔCTD from *epb41l5Δctd* mutants and *epb41l5*-MO^{SpD} morphants. The predicted protein sequence of Epb41l5ΔC60, a translation product of *in vitro* synthesized *epb41l5Δc60* mRNA. Evolutionarily conserved amino acids are shown in red. Peptide sequences originated from mis-splicing of exon 25 and the subsequent frame-shift are shown in blue. (E–J) Gross morphology of homozygous *moe*^{b476} mutant embryos and homozygous *epb41l5Δctd1* mutant embryos at 30 hpf (E–G) and 48 hpf (H–J). Gross morphology of *epb41l5Δctd1* mutants is normal at 30 hpf (F). On the other hand, *moe*^{b476} mutants showed slight body curvature, failure of brain ventricle formation and pericardial edema at 30 hpf (arrowhead in G). At 48 hpf, *epb41l5Δctd1* mutants showed slight body curvature and pericardial edema (arrowhead in I). *moe*^{b476} mutants showed severe body curvature, mosaic eye pigmentation and pericardial edema (arrowhead in J). (K–M) Retinal pigmentation at 48 hpf. *epb41l5Δctd1* mutants did not show the 'mosaic eyes' phenotype (L) as seen in *moe*^{b476} mutants (M). (N-P) Formation of the brain ventricles and apico-basal polarity formation in the hindbrain. In the hindbrain of *epb41l5*-MO^{SpD} morphants, brain ventricle inflation or accumulation of a tight junction protein ZO1 at the ventricular surface was not significantly altered (O) compared to wild type (N). On the other hand, *moe*^{b476} mutants failed to form brain ventricles aligned by ZO1 (P). Scale bars: 100 µm (E–G,K–M), 300 µm (H–J), 50 µm (N–P).

single partial knockdown of either *epb41l5* or *iqcb1* had minimal impacts on embryogenesis in general (Fig. 6Q–S). With partial knockdowns of both *epb41l5* and *iqcb1*, embryos showed LR patterning defects (Fig. 6P). In addition, these double knockdown embryos showed severe body curvature (Fig. 6T,U), previously associated with ciliary dysfunction (Austin-Tse et al., 2013; Becker-Heck et al., 2011; Schottenfeld et al., 2007; Sullivan-Brown et al., 2008). These results suggest that Epb41l5 and Iqcb1 regulate cilia via the same genetic pathway.

EPB41L5 suppresses CEP290 localization to the centrosome

We next explored how EPB41L5 and IQCB1 modulate the integrity of the ciliary base and centrosome. Previous studies showed that IQCB1 interacts with the centrosomal protein CEP290 and that CEP290 is required for IQCB1 localization to the centrosome (Barbelanne et al., 2013; Sang et al., 2011).

We hypothesized that EPB41L5 inhibits IQCB1 interaction with CEP290, leading to IQCB1 dissociation from the centrosome. To test that, we coexpressed EPB41L5, IQCB1 and CEP290 in

Journal of Cell Science (2020) 133, jcs240648. doi:10.1242/jcs.240648

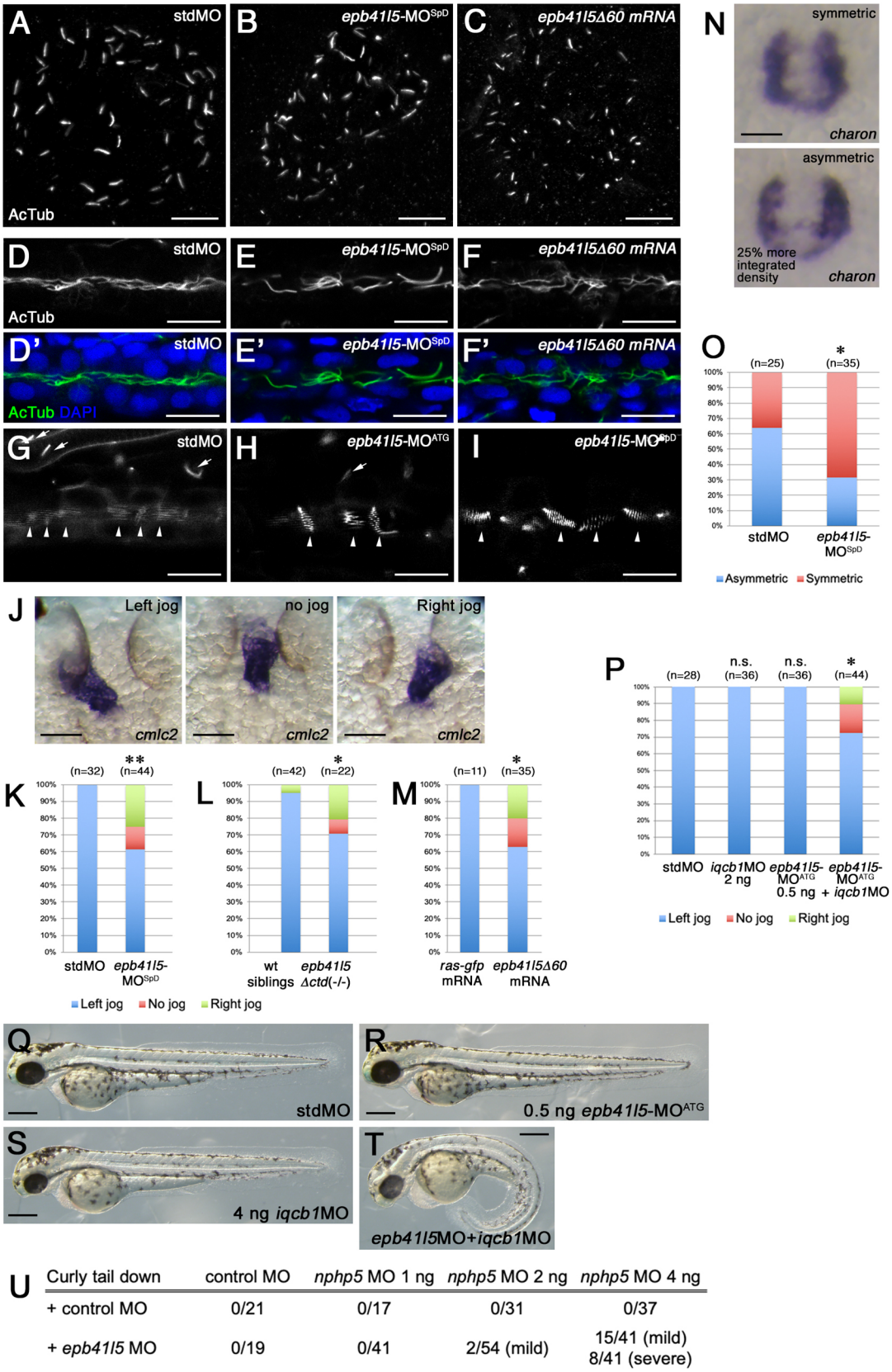

U

Curly tail down	control MO	*nphp5* MO 1 ng	*nphp5* MO 2 ng	*nphp5* MO 4 ng
+ control MO	0/21	0/17	0/31	0/37
+ *epb41l5* MO	0/19	0/41	2/54 (mild)	15/41 (mild) 8/41 (severe)

Fig. 6. See next page for legend.

HEK293 cells for a competitive co-immunoprecipitation assay. First, we confirmed the CEP290–IQCB1 interaction by immunoprecipitation (Fig. 7A,B). EPB41L5 coexpression reduced the overall levels of CEP290 and IQCB1 (Fig. 7C,D), as well as the amount of immunoprecipitated CEP290 (Fig. 7A,D) and IQCB1 (Fig. 7B,D). Nevertheless, EPB41L5 coexpression further reduced

Journal of Cell Science

Fig. 6. Cilia abnormalities in embryos expressing Epb41l5ΔCTD. (A–C) KV cilia formed in control wild-type (stdMO) embryos (A), *epb41l5*-MO^{SpD} morphants (B) and embryos expressing Epb41l5Δ60 (C). KV cilia were immunostained by anti-AcTub antibody at 14 hpf. (D–F′) Pronephric cilia formation. Pronephric cilia were immunostained by anti-AcTub antibody at 32 hpf. Pronephric cilia formed bundles in control wild-type embryos (D,D′). Although cilia formed, individual cilia were easier to distinguish in *epb41l5*-MO^{SpD} morphants (E,E′) and embryos expressing Epb41l5ΔCTD (F,F′). (G–I) Pronephric cilia motility defects in *epb41l5*-MO^{ATD} (H) and *epb41l5*-MO^{SpD} (I) morphants. *epb41l5*-MO^{ATD} or *epb41l5*-MO^{SpD} morpholino were injected into embryos expressing Arl13b-GFP. At 32 hpf, live embryos were mounted in low-melting agarose. Cilia located at the posterior part of the pronephric duct were video-recorded on the confocal microscope with low-speed scanning. In wild-type control embryos (G), the confocal imaging failed to capture the movement of individual cilia, suggesting that cilia motility was high. See Movie 1. (H,I) In *epb41l5*-MO^{ATD} or *epb41l5*-MO^{SpD} morphants, the confocal imaging captured the movement of individual cilia, suggesting that cilia motility is low. See Movies 2 and 3. (J) Representative images of *cmlc2* expression at 28 hpf. The direction of heart jogging was scored as left jog, no jog or right jog. (K–M) LR patterning defects in *epb41l5*-MO^{SpD} morphants (K), *epb41l5Δctd* mutants (L) and embryos expressing exogenous Epb41l5Δ60 (M). (N) Representative image of symmetric or asymmetric *charon* expression in KV. In wild-type embryos, *charon* expression becomes more asymmetric at 14 hpf. (O) *charon* expression was more symmetric in *epb41l5*-MO^{SpD} morphants. Integrated density of *charon* expression in the left side and in the right side was quantified using ImageJ. If integrated density had more than 25% difference, we scored it as asymmetric. (P) Genetic synergy between *epb41l5* and *iqcb1* in LR patterning. The direction of the heart jogging was assessed. Single knockdown of *iqcb1* or *epb41l5* did not alter LR patterning. On the other hand, double knockdown of *iqcb1* and *epb41l5* resulted in LR patterning defects. (Q–T) Genetic synergy between *epb41l5* and *iqcb1* in body curvature. Compared to wild type (Q), single knockdown of *iqcb1* or *epb41l5* did not lead to body curvature (R,S). However, double knockdown of *iqcb1* and *epb41l5* resulted in severe body curvature (T). (U) Quantification of body curvature phenotype in *iqcb1* and *epb41l5* morphants. $^{**}P<0.01$, $^{*}P<0.05$; n.s., not significant. Scale bars: 10 µm (A–I), 100 µm (J), 50 µm (N), 300 µm (Q–T).

the amount of co-immunoprecipitated CEP290 (Fig. 7B,D) and IQCB1 (Fig. 7A,D), supporting our hypothesis. On the other hand, CEP290 coexpression did not reduce the interaction between IQCB1 and EPB41L5 (Fig. 7B).

Additionally, we found that EPB41L5 was co-immunoprecipitated by CEP290 (Fig. 7A), suggesting that EPB41L5 might modulate CEP290 centrosomal localization. This possibility was confirmed in RPE-1 cells (Fig. 7E,F,J). The effect was mediated by the N-terminal FERM-FA domain, but not by the C-terminal fragment of Epb41l5 (Fig. 7G–J). These results show that EPB41L5 displaces both IQCB1 and CEP290 from the centrosome.

DISCUSSION

In this study, we demonstrated a previously uncharacterized role for EPB41L5 in regulating cilia function. Previous work investigated a potential link of EPB41L5 to cilia in mouse *epb41l5* null (*Lulu*) mutants that exhibit LR patterning defects (Lee et al., 2010). Cilia on the left–right organizer are primarily responsible for directional fluid flow generation, and randomized LR patterning is one of the consequences of defects in nodal flow (Basu and Brueckner, 2008; Cartwright et al., 2008; Dasgupta and Amack, 2016). As cilia with normal length formed in the node of *Lulu* mutants, the authors suggested that cilia disfunction in *Lulu* mutant mice is secondary to abnormalities in epithelial morphogenesis of the node. However, their explanation did not rule out the possibility that Epb41l5 has an additional role in cilia.

Zebrafish embryos expressing Epb41l5ΔCTD allowed us to distinguish the roles of Epb41l5 in cilia and epithelial morphogenesis. These embryos maintain largely normal epithelia, although minor epithelial defects contributing to abnormal body curvature and pericardial edema cannot be excluded. We showed that cilia motility and LR patterning were similarly impaired in *epb41l5*-deficient embryos and the embryos expressing Epb41l5ΔCTD. This suggests that Epb41l5ΔCTD maintains its function on epithelial morphogenesis but fails to form or maintain functional cilia.

Our results suggest that EPB41L5 is not required for cilia assembly. Cilia were formed both in *epb41l5*-deficient embryos and embryos expressing Epb41l5ΔCTD. This is consistent with the presence of cilia in mouse *Lulu* mutants (Lee et al., 2010). Nevertheless, EPB41L5 regulates ciliary function. This function of EPB41L5 in cilia appears to be mediated by its interaction with IQCB1 and CEP290. We show that EPB41L5 suppresses the localization of both IQCB1 and CEP290 at the ciliary base and centrosome. We propose that this leads to reduced cilia function, such as reduced cilia motility (Fig. 7K–M). This is also consistent with previous reports on roles of IQCB1 and CEP290 in ciliopathies (Baala et al., 2007; Barbelanne et al., 2013; Coppieters et al., 2010; den Hollander et al., 2006; Helou et al., 2007; Leitch et al., 2008; Otto et al., 2005; Sayer et al., 2006; Valente et al., 2006).

Although we show that EPB41L5 suppresses IQCB1 association with the centrosome, EPB41L5 is probably not the only regulator determining IQCB1 localization at the centrosome. A previous study showed that CEP290 interaction via its C-terminal domain is required for IQCB1 localization to the centrosome (Barbelanne et al., 2013). However, CEP290 interaction appears to be insufficient to localize IQCB1 to the centrosome, because IQCB1 lacking the coiled-coil domain maintains CEP290 binding but failed to localize to the centrosome (Barbelanne et al., 2013). In our experiments, IQCB1 mutants missing the C-terminal CEP290-interacting domain still localized to the centrosome, whereas the localization was weaker than that of full-length IQCB1 (Fig. 3C). Our interpretation is that efficient centrosome localization of IQCB1 requires both the coiled-coil domain and the CEP290-interacting domain. EPB41L5 only regulates IQCB1 association with the centrosome mediated by the coiled-coil domain.

Our study highlights dynamic remodeling of the centrosome and ciliary base under physiological and pathological conditions. We demonstrate that EPB41L5 regulates ciliary function through IQCB1 and CEP290 at the ciliary base and centrosome; however, the details of the underlying mechanism remain unclear. Besides direct effects on IQCB1 and CEP290, EPB41L5 can affect cilia by associating with Mind bomb 1 (MIB1) (Dho et al., 2019; Matsuda et al., 2016), which ubiquitinates CEP290 (Villumsen et al., 2013; Wang et al., 2016). Also, EPB41L5 might regulate cilia through actin remodeling, because actin-targeting drugs restored cilia formation in IQCB1-depleted and CEP290-depleted RPE1 cells (Barbelanne et al., 2013). Additional studies are needed to determine how EPB41L5 affects cilia function.

MATERIALS AND METHODS

Plasmids

Full-length or truncated forms of zebrafish Epb41l5 and mouse EPB41L5 were generated in a previous study (Matsuda et al., 2016). pCBF-FLAG-tagged human IQCB1 was kindly provided by Dr William Tsang (Montreal Clinical Research Institute, Montreal, Canada; Barbelanne et al., 2013). Full-length and truncated forms of IQCB1 were PCR amplified using Choice Taq DNA polymerase (Denville Scientific) and cloned into a pCS2 expression vector using restriction enzymes (New England Biolabs) and the DNA ligation kit, Mightly Mix (Takara). Primers used for PCR amplification are listed in Table S1. Full-length mouse CEP290 (plasmid #27381) was obtained from Addgene. *Not*I and *Stu*I fragments were subcloned into *Not*I and *Sma*I sites of pCS107 expression vector; thereafter, a FLAG tag was inserted into the *Not*I site. Plasmid DNAs were purified using the Qiagen Plasmid Midi kit (Qiagen).

Journal of Cell Science (2020) 133, jcs240648. doi:10.1242/jcs.240648

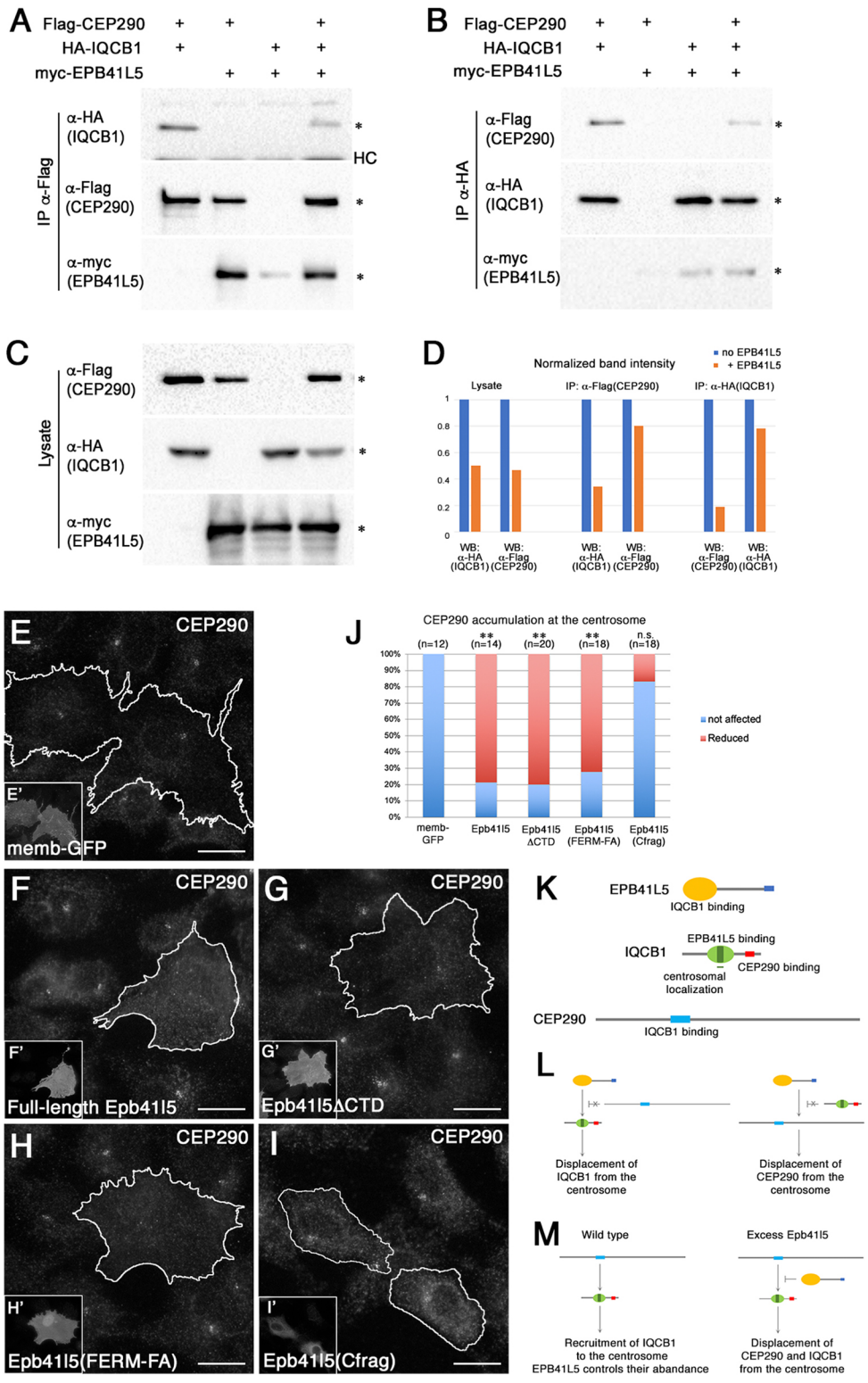

Fig. 7. EPB41L5 overexpression reduces CEP290 accumulation at the centrosome. (A–D) EPB41L5 suppresses the CEP290–IQCB1 interaction. FLAG-CEP290, HA-IQCB1 and myc-EPB41L5 were transiently expressed in HEK293 cells. After 24 h, cell lysates (C) were immunoprecipitated either by anti-FLAG antibody (A) or anti-HA antibody (B). Co-immunoprecipitated proteins and lysate were analyzed by SDS–PAGE and western blotting. EPB41L5 coexpression reduced the amount of HA-IQCB1 co-immunoprecipitated by FLAG-CEP290 (A). EPB41L5 coexpression reduced the amount of FLAG-CEP290 co-immunoprecipitated by HA-IQCB1 (B). (D) Quantification of the band intensities in A–C. Band intensity of HA-IQCB1 and FLAG-CEP290 coexpressed with or without myc-EPB41L5 was quantified. (E–I) EPB41L5 suppresses CEP290 accumulation at the centrosome. Full-length EPB41L5 and deletion mutant forms of EPB41L5 were transiently expressed in hTERT-RPE1 cells. The localization of endogenous CEP290 was examined. Cells expressing memb-GFP (E,E′) or GFP-EPB41L5 (F–I′) were outlined using the Magic Wand tool in Adobe Photoshop. CEP290 localization was not altered in cells expressing control memb-GFP (E). Centrosomal localization of CEP290 was reduced in cells expressing full-length Epb41l5 (F), Epb41l5ΔCTD (G) or Epb41l5(FERM-FA) (H), but was not altered in cells expressing Epb41l5(Cfrag) (I). (J) Quantification of CEP290 accumulation at the centrosome in cells expressing full-length or deletion mutant forms of Epb41l5. CEP290 accumulation was categorized as either not affected or reduced. (K–M) Model showing how EPB41L5 could modulate ciliary function. (K) Summary of domains required for interaction between EPB41L5, IQCB1 and CEP290. Domains for the EPB41L5 and CEP290 interaction have not been identified. (L) EPB41L5 binding to IQCB1 or CEP290 promotes displacement of IQCB1 or CEP290 from the centrosome. Coexpression of either IQCB1 or CEP290 does not inhibit EPB41L5 association with CEP290 or IQCB1, respectively. (M) In wild-type embryos, CEP290 promotes IQCB1 association with the centrosome. Aberrant EPB41L5 activity suppresses IQCB1 and CEP290 interaction, which may further promote displacement of IQCB1 from the centrosome. This may lead to the misplacement of other centrosomal proteins required for ciliary functions, such as cilia motility. $^{**}P<0.01$; n.s., not significant. Scale bars: 10 µm.

Cell culture and transfection

HEK293, hTERT-RPE1 and MDCK cells were purchased from ATCC. HEK293 and MDCK cells were maintained in DMEM (Corning) supplemented with 10% FBS. hTERT-RPE1 cells were maintained in DMEM:F-12 medium (Corning) supplemented with 10% FBS. HEK293, hTERT-RPE1 and MDCK cells were transfected using polyethylenimine (PEI; Polysciences), X-tremeGene HP (Roche) and TransIT-X2 (Mirus), respectively. For cilia formation, cells were grown in serum-free medium for 24 h prior to fixation.

Immunoprecipitation and western blotting

Cell lysates were extracted from HEK293 cells using RIPA buffer (50 mM Tris-HCl pH 7.4, 150 mM NaCl, 1% NP-40, 0.5% sodium deoxycholate, 0.1% SDS) with Protease Inhibitor Cocktail III (Calbiochem). Cell lysates were incubated with primary antibodies (Table S2) and then with protein A/G Sepharose (Santa Cruz Biotechnology) at 4°C for at least 6 h. Sepharose beads were washed in TBST containing 0.05% Triton X-100. Beads were heated at 95°C for 5 min in SDS sample buffer. After SDS–PAGE and transfer to a nitrocellulose membrane with 0.2 µm pore size (GE

Life Sciences), western blots were performed. Antibodies used are listed in Table S2. Chemiluminescent signals were acquired using Clarity ECL Western Blotting Substrates (Bio-Rad) on the ChemiDoc MP Imaging System (Bio-Rad).

Immunostaining of cultured cells

For immunostaining, hTERT-RPE1 cells and MDCK cells were plated on coverslips (Electron Microscopy Sciences) and Transwell (Corning), respectively. Cells were fixed in 4% PFA (Electron Microscopy Sciences) for 15 min at room temperature then permeabilized with 0.1% Triton in PBS for 2 min. After blocking in 1% BSA for 30 min, cells were incubated with primary antibodies (Table S2) for 1 h and then incubated with secondary antibodies conjugated with AlexaFluor 488, AlexaFluor 647 (Invitrogen) or Cy3 (Jackson ImmunoResearch) for 1 h. Immunostained cells were mounted in Mowiol 4-88 (Sigma). Images were acquired on a Nikon A1R confocal microscope or an Olympus BX51 light microscope equipped with an Olympus CCD camera DP73.

Zebrafish maintenance

All zebrafish were maintained and handled according to recommendations in the Guide for the Care and Use of Laboratory Animals of the National Institutes of Health. A protocol for animal use was approved by the Institutional Animal Care and Use Committee (IACUC) at Rutgers University and Ichan School of Medicine at Mount Sinai. AB wild-type fish were obtained from ZIRC. *moe*^{b476} mutants were kindly provided by Dr Monte Westerfield (Institute of Neuroscience, University of Oregon, Eugene, OR; Jensen and Westerfield, 2004). *Tg[bact:arl13b-gfp]* transgenic zebrafish were kindly provided by Dr Brian Ciruna (The Hospital for Sick Children, Toronto, Canada; Borovina et al., 2010). *Tg[dusp:ma-gfp]*^{pt21} zebrafish were kindly provided by Dr Michael Tsang (University of Pittsburgh, Pittsburgh, PA; Molina et al., 2007).

Generation of zebrafish mutants using the CRISPR/Cas9 system

The CRISPR/Cas9 gene editing system was used to generate *epb41l5Δctd* mutants. Three gRNAs (Table S1) were designed to target the splicing donor site of exon 25 in *epb41l5*. gRNAs were generated by oligonucleotide assembly and PCR-based methods (Carrington et al., 2015). The HiScribe T7 Quick High Yield RNA Synthesis kit (New England Biolabs) was used to synthesize gRNAs, which were then purified using Microspin G-25 Columns (GE Healthcare). Cas9 protein was purchased from PNA Bio. gRNA (100 pg) and Cas9 protein (250 pg) were mixed prior to microinjection. The gRNA-Cas9 complex was microinjected into a cell of one-cell stage embryos. At 24 h, genome DNA was extracted to determine the efficacy of gene editing. Primers used for PCR are listed in Table S1.

Microinjection of morpholinos and *in vitro* synthesized mRNA

Morpholino oligonucleotides (Table S1) were purchased from GeneTools (Oregon, USA). *p53* morpholino was co-injected to prevent p53-dependent cell-death and associating off-target effects of morpholinos (Robu et al., 2007). The mMessage mMachine SP6 Transcription kit (Invitrogen) was used to synthesize mRNAs encoding Epb41l5Δ60. Synthesized mRNA was purified by LiCl precipitation. Morpholinos and mRNA were microinjected into the yolk of one- to two-cell stage embryos.

Whole-mount *in situ* hybridization

Ribo probes for *in situ* hybridization were labeled with digoxigenin-UTP (Roche) using SP6, T3 or T7 RNA polymerase (Roche). *In situ* hybridization was performed as described previously (Matsuda and Chitnis, 2009). The BCIP/NBT substrate kit (Vectra lab) was used for coloration. Images were taken on a Leica MZ10 stereomicroscope equipped with an Olympus DP73 CCD camera.

Whole-mount immunocytochemistry

Embryos were fixed in 4% PFA in PBS overnight at 4°C. After permeabilization with 0.1% Triton X-100 for 10 min, embryos were incubated with primary antibodies (Table S2) in 1% BSA in PBS overnight at 4˚C. Embryos were then washed in PBS and incubated with AlexaFluor 488- (Invitrogen) or Cy3-conjugated secondary antibodies (Jackson laboratory) in 1% BSA in PBS overnight at 4°C. After washing with PBS, embryos were transferred into 25, 50 and 75% glycerol in PBS. An A1R confocal microscope system (Nikon) was used for imaging.

Time-lapse imaging of pronephric cilia

Morpholinos were injected into the yolk of one- to two-cell stage *tg[actb: arl13b-gfp]* embryos. At 26–28 hpf, manually dechorinated embryos were mounted in low-melting agarose (Lonza). Time-lapse images were taken on a Nikon A1R confocal microscope system at 5 s intervals for 3 min.

Quantification and statistical analyses

Quantification of fluorescence signals was performed by analyzing individual single plane images. Integrated fluorescence intensity of immunostaining was measured using an ImageJ plugin. The Student's *t*-test was used to test association of continuous variables. When the cell frequency was not equal to zero, the Chi-squared test was used to test categorical variables. When the cell frequency was equal to zero, the Freeman–Halton extension of the Fisher exact probability test was used to test categorical variables.

Acknowledgements

We would like to thank members of the M.M. laboratory for technical assistance and comments on the manuscript. We thank Dr Sergei Sokol for helpful suggestions and editing the manuscript.

Competing interests

The authors declare no competing or financial interests.

Author contributions

Conceptualization: M.M.; Methodology: M.M.; Validation: M.M.; Formal analysis: M.M.; Investigation: T.Y., M.M.; Resources: M.M.; Writing - original draft: M.M.; Writing - review & editing: M.M.; Visualization: M.M.; Supervision: M.M.; Project administration: M.M.; Funding acquisition: M.M.

Funding

This work was supported by the National Institutes of Health (grant R03 HD094980 to M.M. and grant R35 GM122492 to Dr Sergei Sokol). Deposited in PMC for release after 12 months.

Supplementary information

Supplementary information available online at
http://jcs.biologists.org/lookup/doi/10.1242/jcs.240648.supplemental

References

Amack, J. D. and Yost, H. J. (2004). The T box transcription factor no tail in ciliated cells controls zebrafish left-right asymmetry. *Curr. Biol.* **14**, 685-690. doi:10.1016/j.cub.2004.04.002

Amack, J. D., Wang, X. and Yost, H. J. (2007). Two T-box genes play independent and cooperative roles to regulate morphogenesis of ciliated Kupffer's vesicle in zebrafish. *Dev. Biol.* **310**, 196-210. doi:10.1016/j.ydbio.2007.05.039

Austin-Tse, C., Halbritter, J., Zariwala, M. A., Gilberti, R. M., Gee, H. Y., Hellman, N., Pathak, N., Liu, Y., Panizzi, J. R., Patel-King, R. S. et al. (2013). Zebrafish ciliopathy screen plus human mutational analysis identifies C21orf59 and CCDC65 defects as causing primary ciliary dyskinesia. *Am. J. Hum. Genet.* **93**, 672-686. doi:10.1016/j.ajhg.2013.08.015

Avasthi, P., Maser, R. L. and Tran, P. V. (2017). Primary cilia in cystic kidney disease. *Results Probl. Cell Differ.* **60**, 281-321. doi:10.1007/978-3-319-51436-9_11

Avidor-Reiss, T., Ha, A. and Basiri, M. L. (2017). Transition zone migration: a mechanism for cytoplasmic ciliogenesis and postaxonemal centriole elongation. *Cold Spring Harbor Perspect. Biol.* **9**, a028142. doi:10.1101/cshperspect.a028142

Baala, L., Audollent, S., Martinovic, J., Ozilou, C., Babron, M.-C., Sivanandamoorthy, S., Saunier, S., Salomon, R., Gonzales, M., Rattenberry, E. et al. (2007). Pleiotropic effects of CEP290 (NPHP6) mutations extend to Meckel syndrome. *Am. J. Hum. Genet.* **81**, 170-179. doi:10.1086/519494

Baines, A. J. (2006). A FERM-adjacent (FA) region defines a subset of the 4.1 superfamily and is a potential regulator of FERM domain function. *BMC Genomics* **7**, 85. doi:10.1186/1471-2164-7-85

Barbelanne, M., Song, J., Ahmadzai, M. and Tsang, W. Y. (2013). Pathogenic NPHP5 mutations impair protein interaction with CEP290, a prerequisite for ciliogenesis. *Hum. Mol. Genet.* **22**, 2482-2494. doi:10.1093/hmg/ddt100

Barbelanne, M., Hossain, D., Chan, D. P., Peränen, J. and Tsang, W. Y. (2015). Nephrocystin proteins NPHP5 and CEP290 regulate BBSome integrity, ciliary trafficking and cargo delivery. *Hum. Mol. Genet.* **24**, 2185-2200. doi:10.1093/hmg/ddu738

Barker, A. R., Thomas, R. and Dawe, H. R. (2014). Meckel-Gruber syndrome and the role of primary cilia in kidney, skeleton, and central nervous system development. *Organogenesis* **10**, 96-107. doi:10.4161/org.27375

Basu, B. and Brueckner, M. (2008). Multifunctional organelles at the center of vertebrate left-right asymmetry. *Curr. Top. Dev. Biol.* **85**, 151-174. doi:10.1016/S0070-2153(08)00806-5

Becker-Heck, A., Zohn, I. E., Okabe, N., Pollock, A., Lenhart, K. B., Sullivan-Brown, J., McSheene, J., Loges, N. T., Olbrich, H., Haeffner, K. et al. (2011). The coiled-coil domain containing protein CCDC40 is essential for motile cilia function and left-right axis formation. *Nat. Genet.* **43**, 79-84. doi:10.1038/ng.727

Bernabé-Rubio, M. and Alonso, M. A. (2017). Routes and machinery of primary cilium biogenesis. *Cell. Mol. Life Sci.* **74**, 4077-4095. doi:10.1007/s00018-017-2570-5

Borovina, A., Superina, S., Voskas, D. and Ciruna, B. (2010). Vangl2 directs the posterior tilting and asymmetric localization of motile primary cilia. *Nat. Cell Biol.* **12**, 407-412. doi:10.1038/ncb2042

Cao, Y., Park, A. and Sun, Z. (2010). Intraflagellar transport proteins are essential for cilia formation and for planar cell polarity. *J. Am. Soc. Nephrol.* **21**, 1326-1333. doi:10.1681/ASN.2009091001

Carrington, B., Varshney, G. K., Burgess, S. M. and Sood, R. (2015). CRISPR-STAT: an easy and reliable PCR-based method to evaluate target-specific sgRNA activity. *Nucleic Acids Res.* **43**, e157. doi:10.1093/nar/gkv802

Cartwright, J. H. E., Piro, N., Piro, O. and Tuval, I. (2008). Fluid dynamics of nodal flow and left-right patterning in development. *Dev. Dyn.* **237**, 3477-3490. doi:10.1002/dvdy.21672

Carvalho-Santos, Z., Azimzadeh, J., Pereira-Leal, J. B. and Bettencourt-Dias, M. (2011). Tracing the origins of centrioles, cilia, and flagella. *J. Cell Biol.* **194**, 165-175. doi:10.1083/jcb.201011152

Chang, N., Sun, C., Gao, L., Zhu, D., Xu, X., Zhu, X., Xiong, J.-W. and Xi, J. J. (2013). Genome editing with RNA-guided Cas9 nuclease in zebrafish embryos. *Cell Res.* **23**, 465-472. doi:10.1038/cr.2013.45

Chen, J. N., van Eeden, F. J., Warren, K. S., Chin, A., Nusslein-Volhard, C., Haffter, P. and Fishman, M. C. (1997). Left-right pattern of cardiac BMP4 may drive asymmetry of the heart in zebrafish. *Development* **124**, 4373-4382.

Chih, B., Liu, P., Chinn, Y., Chalouni, C., Komuves, L. G., Hass, P. E., Sandoval, W. and Peterson, A. S. (2012). A ciliopathy complex at the transition zone protects the cilia as a privileged membrane domain. *Nat. Cell Biol.* **14**, 61-72. doi:10.1038/ncb2410

Christensen, A. K. and Jensen, A. M. (2008). Tissue-specific requirements for specific domains in the FERM protein Moe/Epb4.1l5 during early zebrafish development. *BMC Dev. Biol.* **8**, 3. doi:10.1186/1471-213X-8-3

Chu, C.-W., Gerstenzang, E., Ossipova, O. and Sokol, S. Y. (2013). Lulu regulates Shroom-induced apical constriction during neural tube closure. *PLoS ONE* **8**, e81854. doi:10.1371/journal.pone.0081854

Coppieters, F., Lefever, S., Leroy, B. P. and De Baere, E. (2010). CEP290, a gene with many faces: mutation overview and presentation of CEP290base. *Hum. Mutat.* **31**, 1097-1108. doi:10.1002/humu.21337

Corbit, K. C., Aanstad, P., Singla, V., Norman, A. R., Stainier, D. Y. R. and Reiter, J. F. (2005). Vertebrate Smoothened functions at the primary cilium. *Nature* **437**, 1018-1021. doi:10.1038/nature04117

Corbit, K. C., Shyer, A. E., Dowdle, W. E., Gaulden, J., Singla, V., Chen, M. H., Chuang, P. T. and Reiter, J. F. (2008). Kif3a constrains β-catenin-dependent Wnt signalling through dual ciliary and non-ciliary mechanisms. *Nat. Cell Biol.* **10**, 497-497. doi:10.1038/ncb1670

Craige, B., Tsao, C.-C., Diener, D. R., Hou, Y., Lechtreck, K.-F., Rosenbaum, J. L. and Witman, G. B. (2010). CEP290 tethers flagellar transition zone microtubules to the membrane and regulates flagellar protein content. *J. Cell Biol.* **190**, 927-940. doi:10.1083/jcb.201006105

D'Angelo, A. and Franco, B. (2009). The dynamic cilium in human diseases. *Pathogenetics* **2**, 3. doi:10.1186/1755-8417-2-3

Das, A., Qian, J. and Tsang, W. Y. (2017). USP9X counteracts differential ubiquitination of NPHP5 by MARCH7 and BBS11 to regulate ciliogenesis. *PLoS Genet.* **13**, e1006791. doi:10.1371/journal.pgen.1006791

Dasgupta, A. and Amack, J. D. (2016). Cilia in vertebrate left-right patterning. *Phil. Trans. R. Soc. B* **371**, 20150410. doi:10.1098/rstb.2015.0410

Dawe, H. R., Smith, U. M., Cullinane, A. R., Gerrelli, D., Cox, P., Badano, J. L., Blair-Reid, S., Sriram, N., Katsanis, N., Attie-Bitach, T. et al. (2007). The Meckel-Gruber Syndrome proteins MKS1 and meckelin interact and are required for primary cilium formation. *Hum. Mol. Genet.* **16**, 173-186. doi:10.1093/hmg/ddl459

Dell, K. M. (2015). The role of cilia in the pathogenesis of cystic kidney disease. *Curr. Opin. Pediatr.* **27**, 212-218. doi:10.1097/MOP.0000000000000187

den Hollander, A. I., Koenekoop, R. K., Yzer, S., Lopez, I., Arends, M. L., Voesenek, K. E. J., Zonneveld, M. N., Strom, T. M., Meitinger, T., Brunner, H. G. et al. (2006). Mutations in the CEP290 (NPHP6) gene are a frequent cause of Leber congenital amaurosis. *Am. J. Hum. Genet.* **79**, 556-561. doi:10.1086/507318

Dho, S. E., Silva-Gagliardi, N., Morgese, F., Coyaud, E., Lamoureux, E., Berry, D. M., Raught, B. and McGlade, C. J. (2019). Proximity interactions of the ubiquitin ligase Mind bomb 1 reveal a role in regulation of epithelial polarity complex proteins. *Sci. Rep.* **9**, 12471. doi:10.1038/s41598-019-48902-x

Downs, L. M., Scott, E. M., Cideciyan, A. V., Iwabe, S., Dufour, V., Gardiner, K. L., Genini, S., Marinho, L. F., Sumaroka, A., Kosyk, M. S. et al. (2016). Overlap of abnormal photoreceptor development and progressive degeneration in Leber congenital amaurosis caused by NPHP5 mutation. *Hum. Mol. Genet.* **25**, 4211-4226. doi:10.1093/hmg/ddw254

Essner, J. J., Amack, J. D., Nyholm, M. K., Harris, E. B. and Yost, H. J. (2005). Kupffer's vesicle is a ciliated organ of asymmetry in the zebrafish embryo that initiates left-right development of the brain, heart and gut. *Development* **132**, 1247-1260. doi:10.1242/dev.01663

Estrada-Cuzcano, A., Roepman, R., Cremers, F. P. M., den Hollander, A. I. and Mans, D. A. (2012). Non-syndromic retinal ciliopathies: translating gene discovery into therapy. *Hum. Mol. Genet.* **21**, R111-R124. doi:10.1093/hmg/dds298

Gamblin, C. L., Parent-Prévost, F., Jacquet, K., Biehler, C., Jetté, A. and Laprise, P. (2018). Oligomerization of the FERM-FA protein Yurt controls epithelial cell polarity. *J. Cell Biol.* **217**, 3853-3862. doi:10.1083/jcb.201803099

Garcia-Gonzalo, F. R., Corbit, K. C., Sirerol-Piquer, M. S., Ramaswami, G., Otto, E. A., Noriega, T. R., Seol, A. D., Robinson, J. F., Bennett, C. L., Josifova, D. J. et al. (2011). A transition zone complex regulates mammalian ciliogenesis and ciliary membrane composition. *Nat. Genet.* **43**, 776-784. doi:10.1038/ng.891

Gerety, S. S. and Wilkinson, D. G. (2011). Morpholino artifacts provide pitfalls and reveal a novel role for pro-apoptotic genes in hindbrain boundary development. *Dev. Biol.* **350**, 279-289. doi:10.1016/j.ydbio.2010.11.030

Goetz, S. C. and Anderson, K. V. (2010). The primary cilium: a signalling centre during vertebrate development. *Nat. Rev. Genet.* **11**, 331-344. doi:10.1038/nrg2774

Gonçalves, J. and Pelletier, L. (2017). The ciliary transition zone: finding the pieces and assembling the gate. *Mol. Cells* **40**, 243-253. doi:10.14348/molcells.2017.0054

Gosens, I., Sessa, A., den Hollander, A. I., Letteboer, S. J. F., Belloni, V., Arends, M. L., Le Bivic, A., Cremers, F. P. M., Broccoli, V. and Roepman, R. (2007). FERM protein EPB41L5 is a novel member of the mammalian CRB-MPP5 polarity complex. *Exp. Cell Res.* **313**, 3959-3970. doi:10.1016/j.yexcr.2007.08.025

Hashimoto, H., Rebagliati, M., Ahmad, N., Muraoka, O., Kurokawa, T., Hibi, M. and Suzuki, T. (2004). The Cerberus/Dan-family protein Charon is a negative regulator of Nodal signaling during left-right patterning in zebrafish. *Development* **131**, 1741-1753. doi:10.1242/dev.01070

Helou, J., Otto, E. A., Attanasio, M., Allen, S. J., Parisi, M. A., Glass, I., Utsch, B., Hashmi, S., Fazzi, E., Omran, H. et al. (2007). Mutation analysis of NPHP6/CEP290 in patients with Joubert syndrome and Senior-Loken syndrome. *J. Med. Genet.* **44**, 657-663. doi:10.1136/jmg.2007.052027

Hildebrandt, F., Attanasio, M. and Otto, E. (2009). Nephronophthisis: disease mechanisms of a ciliopathy. *J. Am. Soc. Nephrol.* **20**, 23-35. doi:10.1681/ASN.2008050456

Hirano, M., Hashimoto, S., Yonemura, S., Sabe, H. and Aizawa, S. (2008). EPB41L5 functions to post-transcriptionally regulate cadherin and integrin during epithelial-mesenchymal transition. *J. Cell Biol.* **182**, 1217-1230. doi:10.1083/jcb.200712086

Hojo, M., Takashima, S., Kobayashi, D., Sumeragi, A., Shimada, A., Tsukahara, T., Yokoi, H., Narita, T., Jindo, T., Kage, T. et al. (2007). Right-elevated expression of charon is regulated by fluid flow in medaka Kupffer's vesicle. *Dev. Growth Differ.* **49**, 395-405. doi:10.1111/j.1440-169X.2007.00937.x

Hoover, K. B. and Bryant, P. J. (2002). Drosophila Yurt is a new protein-4.1-like protein required for epithelial morphogenesis. *Dev. Genes Evol.* **212**, 230-238. doi:10.1007/s00427-002-0231-6

Hsu, Y.-C., Willoughby, J. J., Christensen, A. K. and Jensen, A. M. (2006). Mosaic Eyes is a novel component of the Crumbs complex and negatively regulates photoreceptor apical size. *Development* **133**, 4849-4859. doi:10.1242/dev.02685

Hwang, W. Y., Fu, Y., Reyon, D., Maeder, M. L., Tsai, S. Q., Sander, J. D., Peterson, R. T., Yeh, J.-R. J. and Joung, J. K. (2013). Efficient genome editing in zebrafish using a CRISPR-Cas system. *Nat. Biotechnol.* **31**, 227-229. doi:10.1038/nbt.2501

Ishikawa, T. (2017). Axoneme structure from motile cilia. *Cold Spring Harb. Perspect. Biol.* **9**, a028076. doi:10.1101/cshperspect.a028076

Ishikawa, H. and Marshall, W. F. (2017). Intraflagellar transport and ciliary dynamics. *Cold Spring Harb. Perspect. Biol.* **9**, a021998. doi:10.1101/cshperspect.a021998

Jensen, A. M. and Westerfield, M. (2004). Zebrafish mosaic eyes is a novel FERM protein required for retinal lamination and retinal pigmented epithelial tight junction formation. *Curr. Biol.* **14**, 711-717. doi:10.1016/j.cub.2004.04.006

Jensen, A. M., Walker, C. and Westerfield, M. (2001). mosaic eyes: a zebrafish gene required in pigmented epithelium for apical localization of retinal cell division and lamination. *Development* **128**, 95-105.

Joris, M., Schloesser, M., Baurain, D., Hanikenne, M., Muller, M. and Motte, P. (2017). Number of inadvertent RNA targets for morpholino knockdown in Danio rerio is largely underestimated: evidence from the study of Ser/Arg-rich splicing factors. *Nucleic Acids Res.* **45**, 9547-9557. doi:10.1093/nar/gkx638

Kagan, K. O., Dufke, A. and Gembruch, U. (2017). Renal cystic disease and associated ciliopathies. *Curr. Opin. Obstet. Gynecol.* **29**, 85-94. doi:10.1097/GCO.0000000000000348

Kee, H. L., Dishinger, J. F., Blasius, T. L., Liu, C.-J., Margolis, B. and Verhey, K. J. (2012). A size-exclusion permeability barrier and nucleoporins characterize a ciliary pore complex that regulates transport into cilia. *Nat. Cell Biol.* **14**, 431-437. doi:10.1038/ncb2450

Kim, J., Lee, J. E., Heynen-Genel, S., Suyama, E., Ono, K., Lee, K. Y., Ideker, T., Aza-Blanc, P. and Gleeson, J. G. (2010). Functional genomic screen for modulators of ciliogenesis and cilium length. *Nature* **464**, 1048-1051. doi:10.1038/nature08895

Klena, N. T., Gibbs, B. C. and Lo, C. W. (2017). Cilia and ciliopathies in congenital heart disease. *Cold Spring Harb. Perspect. Biol.* **9**, a028266. doi:10.1101/cshperspect.a028266

Kok, F. O., Shin, M., Ni, C.-W., Gupta, A., Grosse, A. S., van Impel, A., Kirchmaier, B. C., Peterson-Maduro, J., Kourkoulis, G., Male, I. et al. (2015). Reverse genetic screening reveals poor correlation between morpholino-induced and mutant phenotypes in zebrafish. *Dev. Cell* **32**, 97-108. doi:10.1016/j.devcel.2014.11.018

Kramer-Zucker, A. G., Olale, F., Haycraft, C. J., Yoder, B. K., Schier, A. F. and Drummond, I. A. (2005a). Cilia-driven fluid flow in the zebrafish pronephros, brain and Kupffer's vesicle is required for normal organogenesis. *Development* **132**, 1907-1921. doi:10.1242/dev.01772

Kramer-Zucker, A. G., Wiessner, S., Jensen, A. M. and Drummond, I. A. (2005b). Organization of the pronephric filtration apparatus in zebrafish requires Nephrin, Podocin and the FERM domain protein Mosaic eyes. *Dev. Biol.* **285**, 316-329. doi:10.1016/j.ydbio.2005.06.038

Laprise, P., Beronja, S., Silva-Gagliardi, N. F., Pellikka, M., Jensen, A. M., McGlade, C. J. and Tepass, U. (2006). The FERM protein Yurt is a negative regulatory component of the Crumbs complex that controls epithelial polarity and apical membrane size. *Dev. Cell* **11**, 363-374. doi:10.1016/j.devcel.2006.06.001

Law, S. H. W. and Sargent, T. D. (2014). The serine-threonine protein kinase PAK4 is dispensable in zebrafish: identification of a morpholino-generated pseudophenotype. *PLoS ONE* **9**, e100268. doi:10.1371/journal.pone.0100268

Lee, J. D., Silva-Gagliardi, N. F., Tepass, U., McGlade, C. J. and Anderson, K. V. (2007). The FERM protein Epb4.1l5 is required for organization of the neural plate and for the epithelial-mesenchymal transition at the primitive streak of the mouse embryo. *Development* **134**, 2007-2016. doi:10.1242/dev.000885

Lee, J. D., Migeotte, I. and Anderson, K. V. (2010). Left-right patterning in the mouse requires Epb4.1l5-dependent morphogenesis of the node and midline. *Dev. Biol.* **346**, 237-246. doi:10.1016/j.ydbio.2010.07.029

Lee, J. E., Silhavy, J. L., Zaki, M. S., Schroth, J., Bielas, S. L., Marsh, S. E., Olvera, J., Brancati, F., Iannicelli, M., Ikegami, K. et al. (2012). CEP41 is mutated in Joubert syndrome and is required for tubulin glutamylation at the cilium. *Nat. Genet.* **44**, 193-199. doi:10.1038/ng.1078

Leitch, C. C., Zaghloul, N. A., Davis, E. E., Stoetzel, C., Diaz-Font, A., Rix, S., Alfadhel, M., Lewis, R. A., Eyaid, W., Banin, E. et al. (2008). Hypomorphic mutations in syndromic encephalocele genes are associated with Bardet-Biedl syndrome. *Nat. Genet.* **40**, 443-448. doi:10.1038/ng.97

Li, Y. and Hu, J. (2011). Small GTPases and cilia. *Protein Cell* **2**, 13-25. doi:10.1007/s13238-011-1004-7

Li, M., Zhao, L., Page-McCaw, P. S. and Chen, W. (2016). Zebrafish genome engineering using the CRISPR-Cas9 system. *Trends Genet.* **32**, 815-827. doi:10.1016/j.tig.2016.10.005

Linck, R. W., Chemes, H. and Albertini, D. F. (2016). The axoneme: the propulsive engine of spermatozoa and cilia and associated ciliopathies leading to infertility. *J. Assist. Reprod. Genet.* **33**, 141-156. doi:10.1007/s10815-016-0652-1

Liu, Y., Pathak, N., Kramer-Zucker, A. and Drummond, I. A. (2007). Notch signaling controls the differentiation of transporting epithelia and multiciliated cells in the zebrafish pronephros. *Development* **134**, 1111-1122. doi:10.1242/dev.02806

Long, S., Ahmad, N. and Rebagliati, M. (2003). The zebrafish nodal-related gene southpaw is required for visceral and diencephalic left-right asymmetry. *Development* **130**, 2303-2316. doi:10.1242/dev.00436

Lopes, S. S., Lourenco, R., Pacheco, L., Moreno, N., Kreiling, J. and Saude, L. (2010). Notch signalling regulates left-right asymmetry through ciliary length control. *Development* **137**, 3625-3632. doi:10.1242/dev.054452

Loreng, T. D. and Smith, E. F. (2017). The central apparatus of cilia and eukaryotic flagella. *Cold Spring Harb. Perspect. Biol.* **9**, a028118. doi:10.1101/cshperspect.a028118

Madhivanan, K. and Aguilar, R. C. (2014). Ciliopathies: the trafficking connection. *Traffic* **15**, 1031-1056. doi:10.1111/tra.12195

Matsuda, M. and Chitnis, A. B. (2009). Interaction with Notch determines endocytosis of specific Delta ligands in zebrafish neural tissue. *Development* **136**, 197-206. doi:10.1242/dev.027938

Matsuda, M., Rand, K., Palardy, G., Shimizu, N., Ikeda, H., Dalle Nogare, D., Itoh, M. and Chitnis, A. B. (2016). EPB41L5 competes with Delta as a substrate for Mib1 to coordinate specification and differentiation of neurons. *Development* **143**, 3085-3096. doi:10.1242/dev.138743

Mirvis, M., Stearns, T. and James Nelson, W. (2018). Cilium structure, assembly, and disassembly regulated by the cytoskeleton. *Biochem. J.* **475**, 2329-2353. doi:10.1042/BCJ20170453

Mitchison, H. M. and Valente, E. M. (2017). Motile and non-motile cilia in human pathology: from function to phenotypes. *J. Pathol.* **241**, 294-309. doi:10.1002/path.4843

Moleirinho, S., Tilston-Lunel, A., Angus, L., Gunn-Moore, F. and Reynolds, P. A. (2013). The expanding family of FERM proteins. *Biochem. J.* **452**, 183-193. doi:10.1042/BJ20121642

Molina, G. A., Watkins, S. C. and Tsang, M. (2007). Generation of FGF reporter transgenic zebrafish and their utility in chemical screens. *BMC Dev. Biol.* **7**, 62. doi:10.1186/1471-213X-7-62

Nachury, M. V. (2014). How do cilia organize signalling cascades? *Philos. Trans. R. Soc. Lond. B Biol. Sci.* **369**, 20130465. doi:10.1098/rstb.2013.0465

Nakajima, H. and Tanoue, T. (2010). Epithelial cell shape is regulated by Lulu proteins via myosin-II. *J. Cell Sci.* **123**, 555-566. doi:10.1242/jcs.057752

Nakajima, H. and Tanoue, T. (2011). Lulu2 regulates the circumferential actomyosin tensile system in epithelial cells through p114RhoGEF. *J. Cell Biol.* **195**, 245-261. doi:10.1083/jcb.201104118

Nakamura, T., Saito, D., Kawasumi, A., Shinohara, K., Asai, Y., Takaoka, K., Dong, F., Takamatsu, A., Belo, J. A., Mochizuki, A. et al. (2012). Fluid flow and interlinked feedback loops establish left-right asymmetric decay of Cerl2 mRNA. *Nat. Commun.* **3**, 1322. doi:10.1038/ncomms2319

Nigg, E. A. and Raff, J. W. (2009). Centrioles, centrosomes, and cilia in health and disease. *Cell* **139**, 663-678. doi:10.1016/j.cell.2009.10.036

Otto, E. A., Loeys, B., Khanna, H., Hellemans, J., Sudbrak, R., Fan, S., Muerb, U., O'Toole, J. F., Helou, J., Attanasio, M. et al. (2005). Nephrocystin-5, a ciliary IQ domain protein, is mutated in Senior-Loken syndrome and interacts with RPGR and calmodulin. *Nat. Genet.* **37**, 282-288. doi:10.1038/ng1520

Oud, M. M., Lamers, I. J. and Arts, H. H. (2017). Ciliopathies: genetics in pediatric medicine. *J. Pediatr. Genet.* **6**, 18-29. doi:10.1055/s-0036-1593841

Pazour, G. J. and Witman, G. B. (2003). The vertebrate primary cilium is a sensory organelle. *Curr. Opin. Cell Biol.* **15**, 105-110. doi:10.1016/S0955-0674(02)00012-1

Pedersen, L. B. and Rosenbaum, J. L. (2008). Intraflagellar transport (IFT) role in ciliary assembly, resorption and signalling. *Curr. Top. Dev. Biol.* **85**, 23-61. doi:10.1016/S0070-2153(08)00802-8

Perez-Vale, K. Z. and Peifer, M. (2018). Modulating apical-basal polarity by building and deconstructing a Yurt. *J. Cell Biol.* **217**, 3772-3773. doi:10.1083/jcb.201810059

Robu, M. E., Larson, J. D., Nasevicius, A., Beiraghi, S., Brenner, C., Farber, S. A. and Ekker, S. C. (2007). p53 activation by knockdown technologies. *PLoS Genet.* **3**, e78. doi:10.1371/journal.pgen.0030078

Romani, M., Micalizzi, A. and Valente, E. M. (2013). Joubert syndrome: congenital cerebellar ataxia with the molar tooth. *Lancet Neurol.* **12**, 894-905. doi:10.1016/S1474-4422(13)70136-4

Sampaio, P., Ferreira, R. R., Guerrero, A., Pintado, P., Tavares, B., Amaro, J., Smith, A. A., Montenegro-Johnson, T., Smith, D. J. and Lopes, S. S. (2014). Left-right organizer flow dynamics: how much cilia activity reliably yields laterality? *Dev. Cell* **29**, 716-728. doi:10.1016/j.devcel.2014.04.030

Sang, L., Miller, J. J., Corbit, K. C., Giles, R. H., Brauer, M. J., Otto, E. A., Baye, L. M., Wen, X., Scales, S. J., Kwong, M. et al. (2011). Mapping the NPHP-JBTS-MKS protein network reveals ciliopathy disease genes and pathways. *Cell* **145**, 513-528. doi:10.1016/j.cell.2011.04.019

Sayer, J. A., Otto, E. A., O'Toole, J. F., Nurnberg, G., Kennedy, M. A., Becker, C., Hennies, H. C., Helou, J., Attanasio, M., Fausett, B. V. et al. (2006). The centrosomal protein nephrocystin-6 is mutated in Joubert syndrome and activates transcription factor ATF4. *Nat. Genet.* **38**, 674-681. doi:10.1038/ng1786

Schäfer, T., Pütz, M., Lienkamp, S., Ganner, A., Bergbreiter, A., Ramachandran, H., Gieloff, V., Gerner, M., Mattonet, C., Czarnecki, P. G. et al. (2008). Genetic and physical interaction between the NPHP5 and NPHP6 gene products. *Hum. Mol. Genet.* **17**, 3655-3662. doi:10.1093/hmg/ddn260

Schell, C., Rogg, M., Suhm, M., Helmstädter, M., Sellung, D., Yasuda-Yamahara, M., Kretz, O., Küttner, V., Suleiman, H., Kollipara, L. et al. (2017). The FERM protein EPB41L5 regulates actomyosin contractility and focal adhesion formation to maintain the kidney filtration barrier. *Proc. Natl. Acad. Sci. USA* **114**, E4621-E4630. doi:10.1073/pnas.1617004114

Schottenfeld, J., Sullivan-Brown, J. and Burdine, R. D. (2007). Zebrafish curly up encodes a Pkd2 ortholog that restricts left-side-specific expression of southpaw. *Development* **134**, 1605-1615. doi:10.1242/dev.02827

Schulte-Merker, S. and Stainier, D. Y. R. (2014). Out with the old, in with the new: reassessing morpholino knockdowns in light of genome editing technology. *Development* **141**, 3103-3104. doi:10.1242/dev.112003

Schweickert, A., Vick, P., Getwan, M., Weber, T., Schneider, I., Eberhardt, M., Beyer, T., Pachur, A. and Blum, M. (2010). The nodal inhibitor Coco is a critical target of leftward flow in Xenopus. *Curr. Biol.* **20**, 738-743. doi:10.1016/j.cub.2010.02.061

Stainier, D. Y. R., Raz, E., Lawson, N. D., Ekker, S. C., Burdine, R. D., Eisen, J. S., Ingham, P. W., Schulte-Merker, S., Yelon, D., Weinstein, B. M. et al. (2017). Guidelines for morpholino use in zebrafish. *PLoS Genet.* **13**, e1007000. doi:10.1371/journal.pgen.1007000

Stone, E. M., Cideciyan, A. V., Aleman, T. S., Scheetz, T. E., Sumaroka, A., Ehlinger, M. A., Schwartz, S. B., Fishman, G. A., Traboulsi, E. I., Lam, B. L. et al. (2011). Variations in NPHP5 in patients with nonsyndromic leber congenital amaurosis and Senior-Loken syndrome. *Arch. Ophthalmol.* **129**, 81-87. doi:10.1001/archophthalmol.2010.330

Sullivan-Brown, J., Schottenfeld, J., Okabe, N., Hostetter, C. L., Serluca, F. C., Thiberge, S. Y. and Burdine, R. D. (2008). Zebrafish mutations affecting cilia motility share similar cystic phenotypes and suggest a mechanism of cyst formation that differs from pkd2 morphants. *Dev. Biol.* **314**, 261-275. doi:10.1016/j.ydbio.2007.11.025

Takao, D., Wang, L., Boss, A. and Verhey, K. J. (2017). Protein interaction analysis provides a map of the spatial and temporal organization of the ciliary gating zone. *Curr. Biol.* **27**, 2296-2306; e3. doi:10.1016/j.cub.2017.06.044

Tasouri, E. and Tucker, K. L. (2011). Primary cilia and organogenesis: is Hedgehog the only sculptor? *Cell Tissue Res.* **345**, 21-40. doi:10.1007/s00441-011-1192-8

Tepass, U. (2009). FERM proteins in animal morphogenesis. *Curr. Opin. Genet. Dev.* **19**, 357-367. doi:10.1016/j.gde.2009.05.006

Valente, E. M., Silhavy, J. L., Brancati, F., Barrano, G., Krishnaswami, S. R., Castori, M., Lancaster, M. A., Boltshauser, E., Boccone, L., Al-Gazali, L. et al. (2006). Mutations in CEP290, which encodes a centrosomal protein, cause pleiotropic forms of Joubert syndrome. *Nat. Genet.* **38**, 623-625. doi:10.1038/ng1805

Villumsen, B. H., Danielsen, J. R., Povlsen, L., Sylvestersen, K. B., Merdes, A., Beli, P., Yang, Y.-G., Choudhary, C., Nielsen, M. L., Mailand, N. et al. (2013). A new cellular stress response that triggers centriolar satellite reorganization and ciliogenesis. *EMBO J.* **32**, 3029-3040. doi:10.1038/emboj.2013.223

Wang, L., Lee, K., Malonis, R., Sanchez, I. and Dynlacht, B. D. (2016). Tethering of an E3 ligase by PCM1 regulates the abundance of centrosomal KIAA0586/Talpid3 and promotes ciliogenesis. *eLife* **5**, e12950. doi:10.7554/eLife.12950

Wheway, G., Nazlamova, L. and Hancock, J. T. (2018). Signaling through the primary cilium. *Front. Cell Dev. Biol.* **6**, 8. doi:10.3389/fcell.2018.00008

Williams, C. L., Li, C., Kida, K., Inglis, P. N., Mohan, S., Semenec, L., Bialas, N. J., Stupay, R. M., Chen, N., Blacque, O. E. et al. (2011). MKS and NPHP modules cooperate to establish basal body/transition zone membrane associations and ciliary gate function during ciliogenesis. *J. Cell Biol.* **192**, 1023-1041. doi:10.1083/jcb.201012116

Zhao, C. and Malicki, J. (2011). Nephrocystins and MKS proteins interact with IFT particle and facilitate transport of selected ciliary cargos. *EMBO J.* **30**, 2532-2544. doi:10.1038/emboj.2011.165

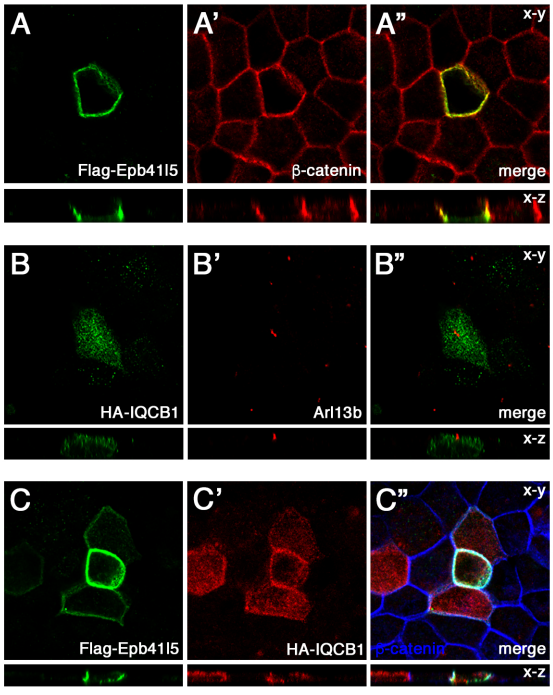

Fig. S1. Subcellular localization of Epb41l5 and IQCB1 in MDCK cells

(A-A") Epb41l5 was localized at the basolateral membrane of MDCK cells. MDCK cells expressing exogenous Flag-Epb41l5 were immunostained by anti-Flag and Adherens Junction (AJ) protein, β-catenin. (B-B") IQCB1 was localized at the apical cytoplasm. MDCK cells expressing exogenous HA-IQCB1 were immiunostained by anti-HA and ciliary protein Arl13b. (C-C") Co-expression of Epb41l5 and IQCB1 in MDCK cells. IQCB1 co-expression did not alter Epb41l5 localization at the basolateral membrane. Epb41l5 co-expression may decrease IQCB1 accumulation in the apical cytoplasm.

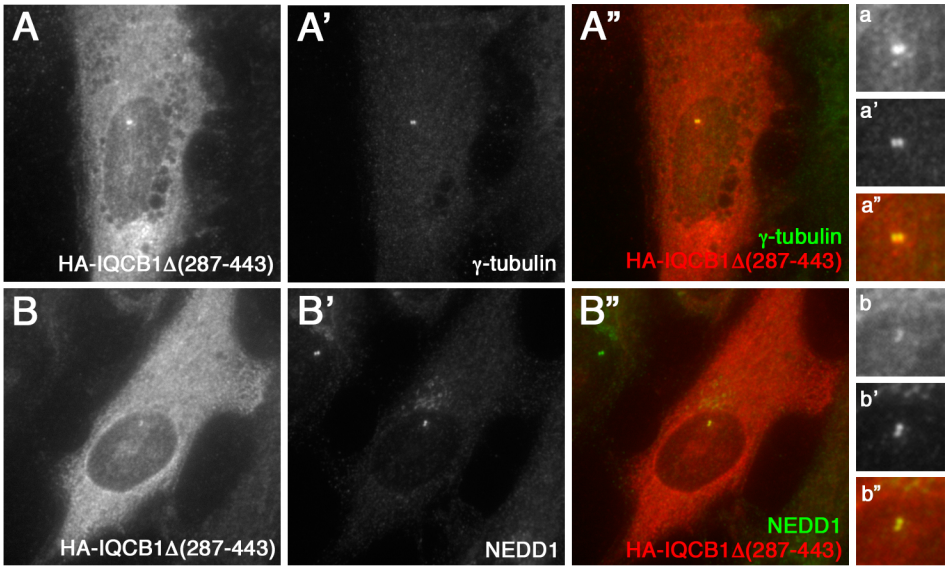

Fig. S2. Subcellular localization of IQCB1Δ(287-443) in in hTERT-RPE1 cells

(A-A") IQCB1Δ(287-443) was co-localized with endogenous γ-tubulin, a centrosome protein. (a-a") Enlarged images of a portion of Fig.S2A. (B-B") IQCB1Δ(287-443) was co-localized with endogenous NEDD1, a centrosome protein. (b-b") Enlarged images of a portion of Fig.S2B.

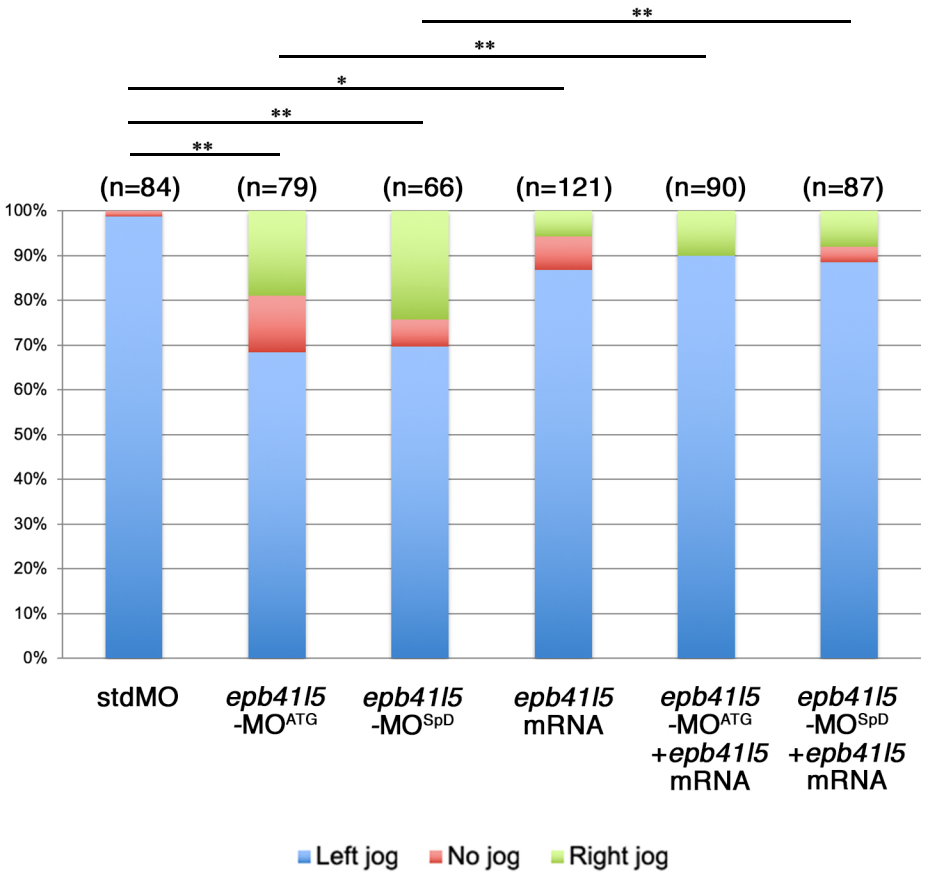

Fig. S3. LR patterning defects in *epb41l5*-MO^{ATG} morphants or *epb41l5*-MO^{SpD} morphants were rescued by co-injection of *epb41l5* mRNA

epb41l5-MO^{ATG} or *epb41l5*-MO^{SpD} morpholinos were injected with or without mRNA encoding full-length Epb41l5 at 1-2 cell stage. The direction of heart jogging at 24 hpf was scored as left jog, no jog or right jog. ** $p<0.01$, * $p<0.05$, n.s. not significant.

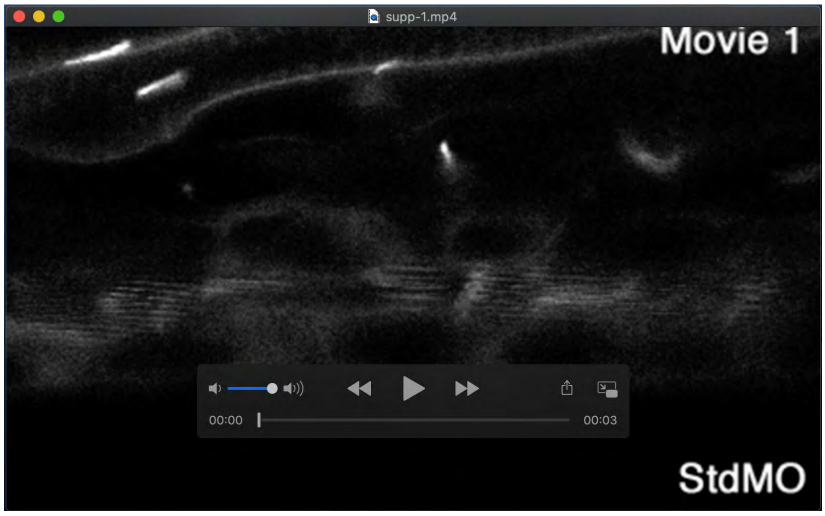

Movie 1. Time-lapse imaging of pronephric cilia in wild-type embryos

Pronephric cilia motility at 28-30 hpf. Images were captured at 5 second intervals for 3 min. Pronephric cilia in control wild-type embryos were difficult to image since them moved much faster than the scanning speed of a conventional confocal microscope. n=5

Movie 2. Time-lapse imaging of pronephric cilia in *epb41l5*-MO^{ATG} morphants. Pronephric cilia motility at 28-30 hpf. Images were captured at 5 second intervals for 3 min. Pronephric cilia in *epb41l5*-MO^{ATG} morphants were more clearly captured compared to wild-type embryos (Movie 1), suggesting that these cilia had reduced motility. n=5

Movie 3. Time-lapse imaging of pronephric cilia in *epb41l5*-MO^{SpD} morphants. Pronephric cilia motility at 28-30 hpf. Images were captured at 5 second intervals for 3 min. Pronephric cilia in *epb41l5*-MO^{SpD} morphants were more clearly captured compared to wild-type embryos (Movie 1), suggesting that these cilia had reduced motility. n=5

Table S1

Name	Sequence (5'-3')	Purposes
hIQCB1-F-BamHI	GGATCCTGAAGCCAACAGGTACAGA	hIQCB1 expression vector
hIQCB1-F1-BamHI-157	GGATCCCTGATTCTCTCTTCTGGC	hIQCB1 expression vector
hIQCB1-R1-XhoI-stop157	CTCGAGTTAAACATGGCCTCCCA	hIQCB1 expression vector
hIQCB1-R2-XhoI-stop290	CTCGAGCTATTCTACTTCCTGATAGAC	hIQCB1 expression vector
hIQCB1-F2-BamHI-287	GGATCCATCAGGAAGTAGAAGAGC	hIQCB1 expression vector
hIQCB1-F3-BamHI-439	GGATCCAGAAACTATTTGCTCCTTG	hIQCB1 expression vector
hIQCB1-R3-XhoI-stop443	CTCGAGTCAAGGAGCAAATAGTTTCT	hIQCB1 expression vector
hIQCB1-R-XhoI-598	CTCGAGCTAAGGTGGTTTGGTTC	hIQCB1 expression vector
hIQCB1Δ(287-443)-F	TCCGACCATTGGGCTTAAAAG	hIQCB1 expression vector
hIQCB1Δ(287-443)-R	GGAGGACTCCAAGAACTC	hIQCB1 expression vector
hEpb41l5-shRNA#1	GAGATGGAACTGGCTATTTTT	hEpb41l5 knockdown in human cell lines
hEpb41l5-shRNA#2	GTTCAGATTCGTGCCTATTCAG	hEpb41l5 knockdown in human cell lines
zEpb41l5 splice donor gRNA 1	GCGTAATACGACTCACTATAGGGGAGAGCAGAAAAGGGTAGCAGTTTTAGAGCTAGAAATAGC	Template oligo for gRNA1 (target sequence is underlined)
zEpb41l5 splice donor gRNA 2	GCGTAATACGACTCACTATAGGGGCAGGGATGAAACAAACCTGGGTTTTAGAGCTAGAAATAGC	Template oligo for gRNA2 (target sequence is underlined)
zEpb41l5 splice donor gRNA 3	GCGTAATACGACTCACTATAGGGGCTCACAATGTCATTGCCACCGTTTTAGAGCTAGAAATAGC	Template oligo for gRNA3 (target sequence is underlined)
zEpb41l5-SpD-F	GCTCTGTTTCCCCTCTTCCT	PCR primer to test gene editing
zEpb41l5-SpD-R	AGGTTTTATTGACCACCAAGC	PCR primer to test gene editing
zEpb41l5-RT-PCR-F	GCTCTGTTTCCCCTCTTCCT	RT-PCR primer
zEpb41l5-RT-PCR-R	GCGTAATACGACTCACTATAGGGGCTCACAATGTCATTGCCACCGTTTTAGAGCTAGAAATAGC	RT-PCR primer
epb41l5-MO-ATG	AGTTTATTCAACTCACCGGCAGGTC	Translation blocking morpholino for zebrafish *epb41l5*
epb41l5-MO-SpD	TAGCAGGGATGAAACAAACCTGGT	Splicing blocking morpholino for zebrafish *epb41l5*
iqcb1-MO	TCAAATCTGAATACCTGAGGAGGTC	Splicing blocking morpholino for zebrafish *iqcb1*
tp53-MO	GCGCCATTGCTTTGCAAGAATTG	morpholino for *p53*

Table S2

Name	Manufacture	Catalog number	Dilution
Primary antibodies			
rat anti-HA (clone 3F10)	Roche	11867423001	1/100 (IF)
mouse anti-HA (clone 16B12)	Covance	MMS-101P	1/300 (IF) 1/2000 (WB)
mouse anti-Flag (clone 2H8)	Cosmo Bio	KAL-KO602	1/500 (IF) 1/2000 (WB)
mouse anti-AcTub (clone 6-11B-1)	Sigma Aldrich	T7451	1/300 (IF)
rabbit anti-myc	Sigma Aldrich	C3956	1/500 (IF) 1/2000 (WB)
rabbit anti-Arl13b	Proteintech	17711-1-AP	1/500 (IF) 1/2000 (WB)
rabbit anti-γ-Tubulin	Abcam	ab11321	1/300 (IF)
mouse anti-NEDD1	Abnova	H00121441-MO5	1/300 (IF)
rabbit anti-β-catenin	Sigma Aldrich	PLA0230	1/500 (IF)
Secondary antibodies			
HRP anti-mouse IgG	Cell Signaling	7074	1/3,000 (WB)
HRP anti-rabbit IgG	Cell Signaling	7076	1/3,000 (WB)
Alexa Fluor 488 anti-rabbit IgG	Invitrogen	A-11034	1/200 (IF)
Alexa Fluor 488 anti-mouse IgG	Invitrogen	A-11029	1/200 (IF)
Alexa Fluor 647 anti-rabbit IgG	Invitrogen	A-21245	1/200 (IF)
Cy3 anti-mouse IgG	Jackson ImmunoResearch	715-165-151	1/500 (IF)
Cy3 anti-rabbit IgG	Jackson ImmunoResearch	711-165-152	1/500 (IF)
Cy3 anti-rat IgG	Jackson ImmunoResearch	712-165-153	1/500 (IF)